embryonic day 14.5 Balb/c mouse embryos as described (*18*). MEFs were cultured in DMEM medium supplemented with non-essential amino acids plus 1 mM pyruvic acid (Invitrogen, Carlsbad, CA, USA) and 10% heat-inactivated FBS. Stably transformed Colon 26 cells were cultured in RPMI 1640 medium supplemented with 300 μg/ml geneticin (Invitrogen). All media were supplemented with 100 U/ml penicillin (Invitrogen), and 100 μg/ml streptomycin (Invitrogen).

Cell Proliferation Assay Using Multi-drug Resistance Transporter Inhibitor—Cell proliferation was determined by WST-8 reagent (Dojindo, Kumamoto, Japan) under the manufacturer's instruction. This assay is basically similar to the 3-[4,5-dimethylthiazol-2-yl]-2,5-diphenyltetrazolium bromide (MTT) assay. Cells were seeded at a density of 3×10^3 cells per well in 96-well plates, and after overnight cultivation, Cyclosporine A (CyA; Wako, Osaka, Japan) of concentrations ranging from 1 to 10 μM or 20 M reserpine (Rs; Sigma) was added to wells. After 48 h of incubation with drug, WST-8 reagent was added to each well and cells were incubated for an additional 2 h. Absorbance at 405 nm was determined using a Biotrac II platereader (Amersham biosciences, Piscataway, NJ, USA).

Transient Knockdown of mdr1a/1b—Transient knockdown of *mdr1a/1b* gene of Colon 26 and B16 cells was performed using the short hairpin RNA (shRNA) method. shRNA coding for *mdr1a/1b* was inserted into the pSINsi-hU6 DNA vector (Takara, Shiga, Japan) at the BamH1 and Cla1 ligation sites according to the manufacturer's instruction. shRNA oligonucleotides were synthesized corresponding to the published sequence of *mdr1a* and *mdr1b* mRNAs (*mdr1a*: NM_011076, *mdr1b*: NM_011075). The following specific DNA inserts were used: *mdr1a/1b* shRNA (insert 1; forward strand: 5′-gatcc GTG TGT TCA TAG TTG TCT ATA ttc aag aga TGT AGG CAA CTA TGA GCA CAC tttttt at-3′, reverse strand: 5′-cgat aaaaaa GTG TGC TCA TAG TTG CCT ACA tct ctt gaa TAT AGA CAA CTA TGA ACA CAC g-3′), (insert 2; forward strand: 5′-gattc GAT CGT TGG TGT GGT GGG TCG ttc aag aga TGA CTC ACC ACA CCA ATG ATC tttttt at-3′, reverse strand: 5′-cgat aaaaaa GAT CAT TGG TGT GGT GAG TCA tct ctt gaa CGA CCC ACC ACA CCA ACG ATC g-3′) and a non-specific oligonucleotide insert for negative control (forward strand: 5′-gatcc GAT CGT TGG TGT GGT GGG TCG ttc aag aga ACT ACC ATG CTC CCA TGA ACA tttttt at-3′, reverse strand: 5′-cgat aaaaaa TGT TCA TGG GAG CAT GGT AGT tct ctt gaa CGA CCC ACC ACA CCA ACG ATC g-3′). Colon 26 and B16 cells were seeded at a density of 3×10^5 cells per well in 24-well plates. The following day, a plasmid containing one of the DNA inserts (noted above) was transfected into the cells using lipofectamine 2000 reagent (Invitrogen) according to the manufacture's instruction. For the evaluation of *mdr1a/1b* knockdown, *mdr1a/1b* expression was determined by real-time reverse transcription (RT) and polymerase chain reaction (PCR) (RT-PCR) and immunoblotting. Total RNA, for real-time RT-PCR, was collected from cells 48 h after transfection. Total cell lysate for immunoblotting was prepared from cells after 72 h of transfection. For growth assay, transfected cells were harvested with trypsin and re-seeded at a density of 3×10^4 cells in 6-well plates after 1 day of transfection. Four days later, cells were harvested and the total cell number was determined.

Generation of mdr1a/1b Knockdown Cells—Stable knockdown of *mdr1a/1b* gene of Colon 26 cells was achieved using the shRNA. shRNA vectors with mdr1a/1b-specific insert 1, non-specific insert or a mock vector was used. Colon 26 cells were seeded at a density of 1×10^4 cells per well in 24-well plates. The following day, a plasmid containing the DNA insert (noted above) was transfected by using lipofectamine 2000 reagent (Invitrogen) using the manufacture's instruction. Forty-eight hours after infection, the cells were harvested by trypsinization and re-seeded at a density of 2×10^4 cells in 10-cm culture dishes. The following day, geneticine was added to a final concentration of 300 μg/ml. Eight days after addition of geneticine, colonies were picked by using a cloning ring (Asahi techno glass corporation, Tokyo, Japan) and re-seeded in the culture plate. For the evaluation of *mdr1a/1b* knockdown, *mdr1a/1b* expression was determined by real-time RT-PCR.

RNA Isolation and RT-PCR Analysis—Total RNA was collected using Isogen reagent (Invitrogen) as previously reported (*19*). Total RNA was reverse transcribed using the MMLV Reverse Transcriptase (Invitrogen). The cDNA was amplified using *Taq* polymerase (Takara) in a GeneAmp PCR system model 9700 (Applied Biosystems, Foster City, CA, USA) using 32 cycles. Each cycle consisted of denaturation at 94 C for 1 min, annealing at 60 C for 1 min and extension at 72 C for 1 min. Primers used for RT-PCR were as follows; *mdr1a* (sense: GAA TTG GTG ACA AAA TCG GA, anti-sense: TGT CTA TAC TGG GCT TAT TA), *mdr1b* (sense: GGA ACT CTC GCT GCT ATT AT, anti-sense: GGT TAG CTT CCA ACC ACT TA), *mdr2* (sense: AAC ACA GCC AAC CTT GGA AC, anti-sense: CAG CCC TTC TCC ACT GTA GC), *mrp1* (sense: CCA CTC TGG GAC TGG AAT GT, anti-sense: GGG GTG AGC AGT CTG AGA AG), *beta-actin* (sense: CCT AAG GCC AAC CGT GAA AAG, anti-sense: TCT TCA TGG TGC TAG GAG CCA).

For real-time RT-PCR, reactions were performed by using platinum SYBR green qPCR supermix UDG reagent (Invitrogen). Cycling conditions were 2 min at 50 C, 10 min at 95 C, followed with 41 cycles of alternating 15 s at 95 C and 1 min at 60 C. The quantity of *mdr1a*, *mdr1b*, *mrp1* detected in each reaction tube was normalized to the level of the glyceraldehyde 3-phosphate dehydrogenase (*GAPDH*) internal control. Primers used for real-time RT-PCR were as follows; *mdr1a* (sense: AGT GTC AGC ATC CCA CAT CA, anti-sense: TTG CAC ATT TCC TTC CAA CA), *mdr1b* (sense: GGA CAT CCT TGG TCC TCT CA, anti-sense: CTA TGT TTG GGG CCA AGT GT), *mrp1* (sense: TTG GTG TGA GCT GGT CTC TG, anti-sense: TTT GGG TTT TGT CTG GGA AG), *GAPDH* (sense: TGG CAA AGT GGA GAT TGT TGC C, anti-sense: AAG ATG GTG ATG GGC TTC CCG). Data were collected using an ABI prism 7900 HT RT-PCR System (Applied Biosystems).

Immunoblotting—Total cell lysates from each transfectant were prepared by lysis in buffer [10 mM Tris–HCl

(pH7.4), 1% NP-40, 0.1% sodium deoxycholate, 0.1% SDS, 0.15 M NaCl, 1 mM EDTA-2Na] and the proteins were separated by electrophoresis on 10% polyacrylamide gels containing SDS. The proteins were transferred by electroblotting to polyvinylidene difluoride membranes and the membranes were subsequently incubated with the following antibodies: anti p-gp rabbit polyclonal antibody (H-241; Santa Cruz, DE, CA, USA), anti GAPDH mouse monoclonal antibody (Chemicon, Temecula, CA, USA), anti-extracellular signal-regulated kinase 1/2 (ERK1/2) rabbit polyclonal antibody or anti-phospho-ERK1/2 (Thr202/Thr204) rabbit polyclonal antibody (Cell Signaling Technology, Beverly, MA). Proteins were detected with horseradish peroxidase (HRP)-conjugated anti-rabbit Ig (Dako Cytomation, Glostrup, Denmark), anti-mouse Ig (Dako) or anti-rabbit IgG (Cell Signaling Technology, for detection of P-ERK1/2). After extensive washing, the antigen was visualized using the ECL plus reagents (Amersham) according to the manufacturer's instructions.

Cell Kinetics Assays Using Mdr1 Knockdown Cell Line—For cytotoxicity assay, cells were seeded at a density of 3×10^3 cells per well in 96-well plate, and next day 0.5 μg/ml doxorubicin (DXR; Biovision, Mountain View, CA, USA) was added. After 48 h of incubation with drug, WST-8 reagent was added to each well and cells were incubated for an additional 2 h. Absorbance at 405 nm was determined using a Biotrac II plate reader (Amersham Biosciences). For cell growth assay, each clone was seeded at a density of 5×10^4 cells per well in 6-well plates. The following day and 3 days later, cells were collected by trypsinization, counted by using a cell counting chamber and the doubling time for cell division was calculated. For the analysis of DNA synthesis, each clone was seeded at a density of 3×10^4 cells per well in 24-well plates. Two days later, bromodeoxyuridine (BrdU; SIGMA) was added at 10 μM, and incubated for 4–5 h. To examine BrdU positive cell, cells were incubated with anti-BrdU rat IgG (abcam, Cambridge, Cambridgeshire, UK), followed with alexa 488-conjugated goat anti rat IgG antibody (molecular probes, Eugene, OR, USA), and examined by fluorescence microscopy (IX70, Olympus, Tokyo, Japan). For nuclear counter staining, Hoechst 33342 (Nacalai, Kyoto, Japan) was used. Immunocytochemical methods were performed as described previously (*20*). For cell cycle analysis, each clone was seeded at a density of 5×10^5 cells per 10-cm culture dishes. Two days later, cells were collected and stained with propidium iodide (PI) using standard protocol. Stained cells were detected by flow cytometry, FACS calibur system (Becton Dickinson, Franclin Lakes, NJ, USA), and analysed by Modfit LT software (Verity Software House, Augusta, ME, USA).

Mouse Xenograft Assay—Six- to 8-week-old female Balb/c mice were injected subcutaneously with 5×10^5 cells as described previously (*19*). Mice injected with cells were sacrificed 2 weeks post-injection, the tumour was dissected and the tumour weight was determined. Mice were purchased from SLC (Shizuoka, Japan). These studies were approved by the animal care committee of Osaka University and Kanazawa University.

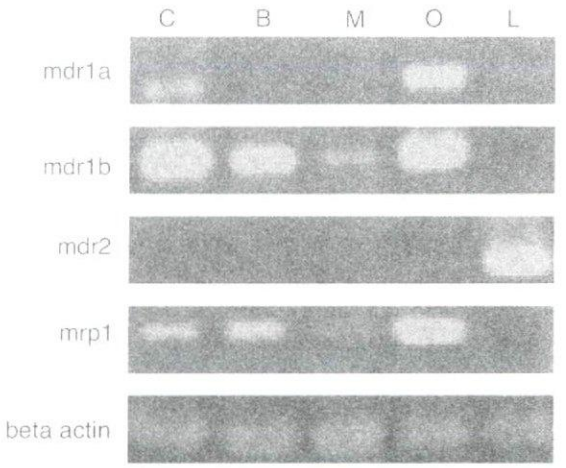

Fig. 1. **Expression of *mdr1a/1b* mRNA in tumour cells.** Total RNA from each cell type was subjected to RT-PCR analysis. C: Colon 26, B: B16 melanoma, M: MEFs, O: OP9, L: mouse whole liver. Liver was used as positive control for mdr2 detection; beta-actin was used as an internal control.

RESULTS

Suppression of Tumour Cell Proliferation by Inhibition of Mdr1 Function—Intestinal tumourigenesis usually observed in Min ($Apc^{Min/+}$) mice was reported to be suppressed in the *mdr1a/1b* double mutant background (*17*). This might suggest that malignant proliferation of tumour cells is dependent on Mdr1a/1b function. To test this property, we observed *mdr1a/1b* expression on cells from a mouse colon cancer cell line, Colon 26, and compared its expression to that on cells from a non-gastrointestinal cancer cell line, B16 (melanoma), osteoblastic cell line OP9 and primary normal cells, MEFs. As expected, Colon 26 cells expressed both *mdr1a* and *mdr1b* (Fig. 1). On the other hand, B16 melanoma cells and MEFs expressed *mdr1b* weakly but did not express *mdr1a*. Moreover, OP9 cells expressed both *mdr1a* and *mdr1b* as found in Colon26 cells. To test the role of Mdr1 in cell proliferation, firstly, we blocked the pump function of Mdr1 on these four different types of cells by using MDR modifier CyA or Rs. MEFs and OP9 cells could proliferate in the presence of increasing concentrations (up to 10 μM) of CyA but the growth of Colon 26 and B16 cells decreased by as much as 70–80% at the highest concentration (Fig. 2A). As with CyA, Rs suppressed the growth of Colon 26 and B16 cells but not that of MEFs. However, unlike CyA, Rs attenuated the proliferation of OP9 cells (Fig. 2B). These results suggested that MDR1 function is associated with proliferation of transformed cells that had acquired the property of permanent cell proliferation, like tumour cells. However, based on controversial result of CyA and Rs on the growth of OP9 cells, it appears that gene knockdown experiment of Mdr1 is required for the clarification of whether Mdr1 is actually involved in tumour cell growth or not. Moreover, there is another member of a multi-drug resistance transporter family of proteins Mrp1. Mrp1 is expressed on tumour cells and CyA also inhibit Mrp1 pump function (*5*). Indeed, both colon 26 cells and B16 melanoma cells expressed *mrp1* (Fig. 1). Therefore, to

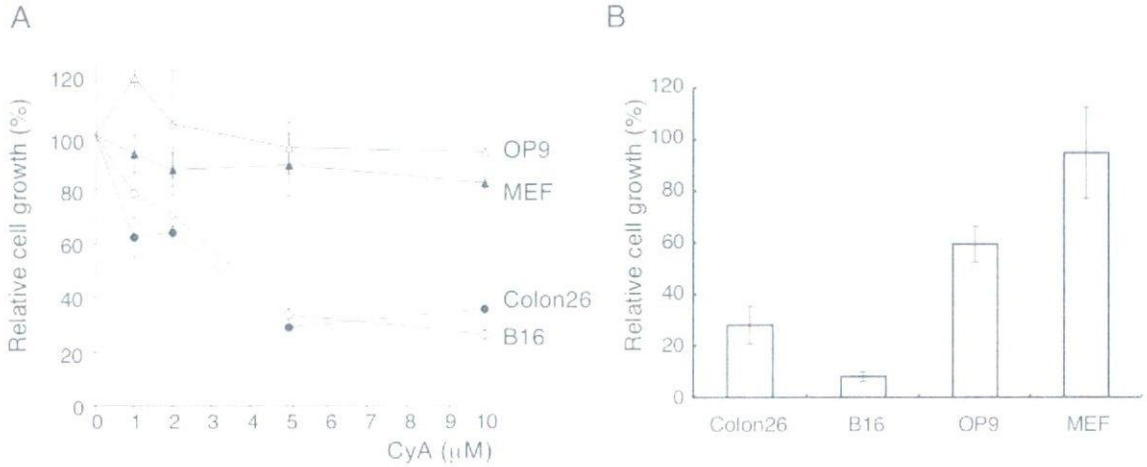

Fig. 2. **Effect of *mdr1a/1b* on cell growth.** (A) After 2 days of culturing with various concentration of CyA as indicated, cell growth was analysed with WST-8 assay. For each concentration of CyA, the percentage of O.D. measured in the presence of CyA relative to that in the absence of CyA is shown. Filled circle: Colon 26 cells, open circle: B16 cells, filled triangle: MEFs, open triangle: OP9. Each data point represents the mean and the bar shows the SD of three independent measurements. (B) After 2 days of culturing with 20μM reserpin (Rs), cell growth was analysed using the WST-8 assay. The percentage of O.D. measured in the presence of Rs relative to that in the absence of Rs is shown.

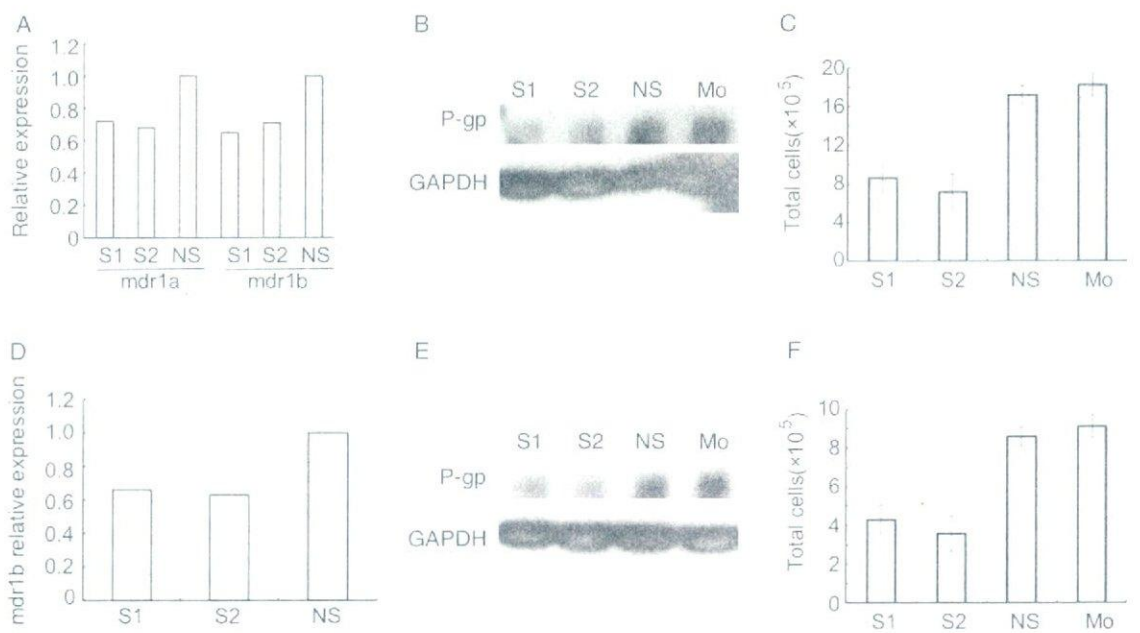

Fig. 3. **Effect of transient mdr1a/1b knockdown on tumour cell growth.** After transfection with S1 or S2 (two different vector containing shRNA for mdr1a/1b), NS (vector containing a non-specific insert) or Mo (mock vector containing no shRNA insert) into Colon 26 cells (A–C) or B16 cells (D–F), expression of mRNA for *mdr1a/1b* was determined (A, D) and protein level (B, E) and cell growth was measured in the cell cultures (C, F). (A and D) Total RNA from cells transfected with each vector was subjected to real-time RT-PCR analysis. Data show the relative expression level of *mdr1a* or *mdr1b* (A) or *mdr1b* (D) gene in S1 or S2 transfected cells compared with that in NS transfected cells. (B and E) Total protein from cells transfected with each vector was subjected to western blotting analysis. p-gp and GAPDH expression of the clones was analysed. GAPDH was used as an internal control. (C and F) Cells transfected with each vector were seeded in culture dishes; the total number of cells was determined after 4 days of culturing. Data show mean ± SD derived from representative result of three independent experiments.

test whether growth inhibition of tumour cells is actually regulated by *mdr1a/1b*, we ablated *mdr1a/1b* genes in Colon 26 and B16 cells by performing RNA interference (RNAi).

Transient Knockdown of mdr1a/1b Gene on Colon26 and B16 Cells Inhibits Cell Growth—To test whether attenuation of mdr1a/1b expression on Colon 26 or B16 cells inhibits cell growth or not, we performed gene silencing by using shRNA method (Fig. 3). Mice express two genes encoding *Mdr1*, *mdr1a* and *mdr1b* (*12*). In humans, a single MDR1 product displays both functions of murine Mdr1a and Mdr1b (*13*). Mouse *mdr1a* is

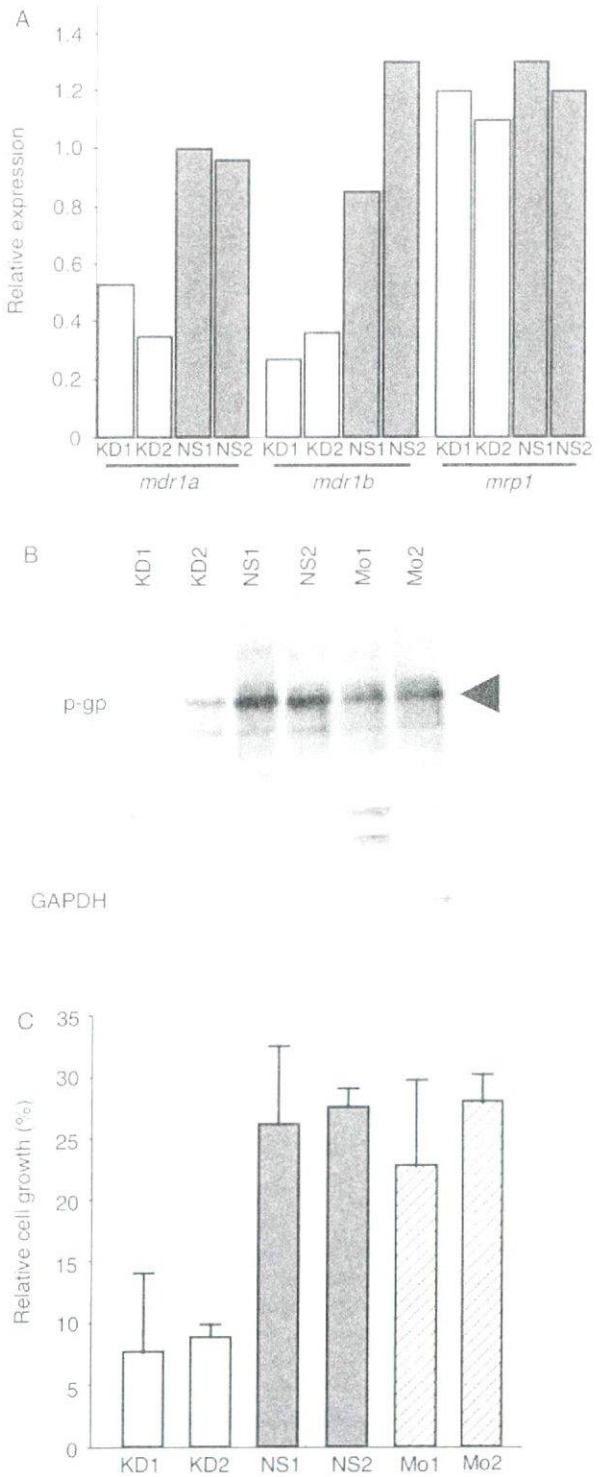

Fig. 4. **Generation of stable *mdr1a/1b* knockdown Colon26 cells.** (A) Total RNA from each clones were subjected to real-time RT-PCR analysis. Data show the relative expression level of RNA compared to Colon 26 clones transfected with a mock vector. In each clone, *mdr1a*, *mdr1b* and *mrp1* expression were analysed. (B)Total protein from each clone was subjected to western blotting analysis. p-gp and GAPDH expression of the clones were analysed. GAPDH was used as an internal control. (C) To evaluate the suppression of *mdr1a/1b*, each clone was incubated with 0.5 μg/ml DXR. Two days later after incubation with DXR, cell growth was analysed by WST-8 assay. Data represent relative ratio of O.D. from cells incubated with DXR compared with that incubated with control vehicle. Data show mean ± SD ($n = 3$) derived from representative result of three independent experiments. KD1, KD2: 2 independent clones of *mdr1a/1b* knockdown Colon 26 cells using *mdr1a/1b*-specific shRNA; NS1, NS2: 2 independent clones of control Colon 26 cells transduced with a vector containing a non-specific shRNA insert; Mo1, Mo2: 2 independent clones of control Colon 26 cells transduced with a mock vector containing no shRNA insert.

expressed in the intestinal epithelium and at the blood–brain and blood–testis barriers, whereas *mdr1b* is highly expressed in the adrenal gland, pregnant uterus and ovary. Although tissue distribution of *mdr1a* or *mdr1b* is different, functional discrimination between *mdr1a* and *mdr1b* has not been reported (*15*). Therefore, in order to know the function of Mdr1 in tumour cells, we used plasmids containing two different oligonucleotide inserts of shRNA (S1 or S2) that specifically recognize both of *mdr1a* and *mdr1b* sequences. With this method, we caused interference with the expression of *mdr1a* and *mdr1b* by using a common sequence shared by both *mdr1a* and *mdr1b* mRNAs. Upon transfection with plasmids (S1 and S2), both *mdr1a* and *mdr1b* expression of Colon 26 cells and *mdr1b* expression on B16 cells were reduced compared with the level of expression of control cells transfected with a plasmid containing a non-specific shRNA (NS) (Fig. 3A and D). Western blotting showed a reduction in mdr1a/1b (p-gp) protein expression in Colon 26 and B16 cells transfected with S1 or S2 containing vectors (Fig. 3B and E). Under these conditions of reduced mdr1a/1b expression, suppression of tumour cell growth was observed in both Colon 26 and B16 cells (Fig. 3C and F). Therefore, we confirmed that inhibition of pump function of tumour cells suppresses cell proliferation.

Stable Knockdown of mdr1a/1b Genes on Colon 26 Cells Inhibits Cell Growth—Finally, as it has been reported that intestinal tumourigenesis observed in Min ($Apc^{Min/+}$) mice was suppressed in the *mdr1a/1b* double mutant background (*17*), we tested how attenuation of mdr1a/1b expression affects *in vitro* and *in vivo* cell growth of Colon 26 intestinal cancer cells, when *mdr1a/1b* genes were stably knocked down in these cells.

Upon transfection with plasmids containing shRNA oligonucleotides (specific insert 1) that specifically recognized *mdr1a/1b* sequences, both *mdr1a* and *mdr1b* expression of Colon 26 cells (KD1 and KD2, two different subclones) was reduced compared to the level of expression when the cells were transfected with a plasmid containing non-specific shRNA (NS1 and NS2); however, expression of *mrp1* was not affected by this RNAi method (Fig. 4A). Western blotting showed a reduction in mdr1a/1b (p-gp) protein expression in clones (KD1 and KD2, two different subclones) (Fig. 4B), as found in the real-time PCR analyses for mRNA expression.

Using several independent knockdown transformants of Colon 26 cells (KD1 and KD2), we evaluated the sensitivity for anti-cancer drug, DXR, to confirm whether Mdr1a/1b function was reduced by the RNAi method. As showed in Fig. 4C, sensitivity for DXR was not affected in Colon 26 subclones transduced with non-specific shRNA (NS1 and NS2) and also with mock vector

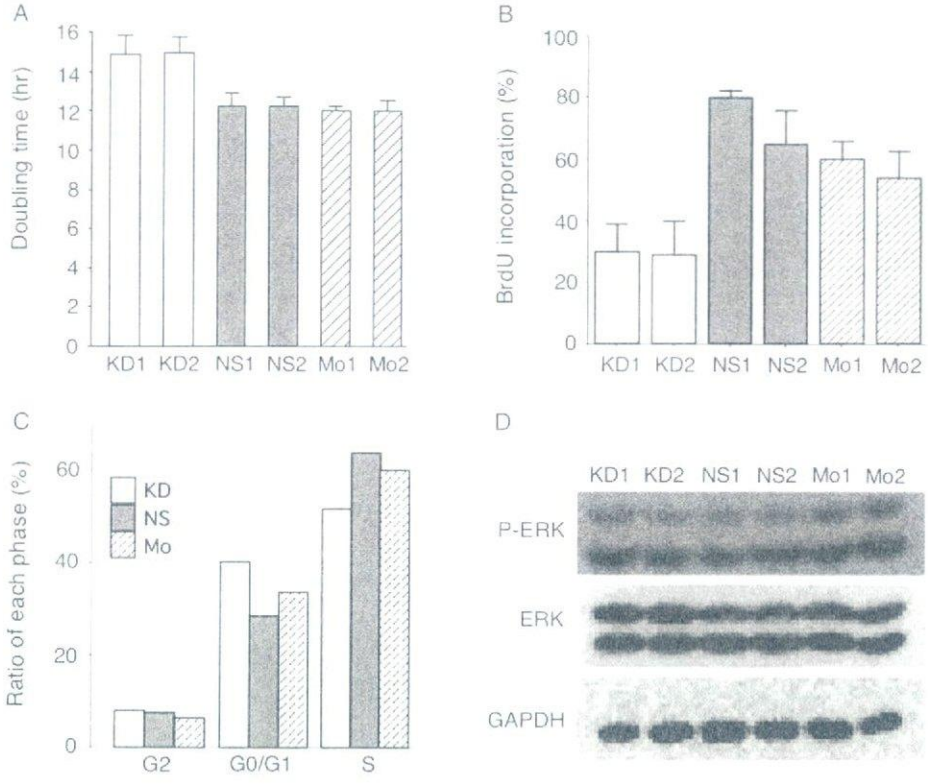

Fig. 5. **Knockdown of *mdr1a/1b* inhibits growth activity of tumour cells.** (A) Cell growth was affected by knockdown of *mdr1a/1b* on Colon 26 cells. Cells were seeded in culture dishes; the total number of cells was determined on Day 1 and Day 3 and the doubling time for cell division was calculated. Data shows doubling time; data represent the mean ± SD of three experiments ($n = 3$). (B) DNA synthesis affected by knockdown of *mdr1a/1b* on Colon 26 cells. Clones were seeded in culture dishes and 2 days later BrdU was added to the culture. Data show percentage of BrdU-positive cells/total cells. Bar graphs show the mean and the bar lines show the SD ($n = 3$). (C) Cell cycle was affected by knockdown of *mdr1a/1b* of Colon 26 cells. Cells were stained with PI and analysed by flowcytometry. The percentage of cells in G2, G0/1 and S phase are shown. Data are representative results from three independent experiments. (D) Total protein from each clone was subjected to western blotting analysis. P-ERK, ERK and GAPDH expression of the clones was analysed. GAPDH was used as an internal control. KD; *mdr1a/1b* knockdown Colon 26 cells using mdr1a/1b specific shRNA, NS; control Colon 26 cell transduced with a non-specific insert, Mo; control Colon 26 cells transduced with a mock vector. Numerals 1 and 2 for KD, NS and Mo in (A, B) indicate two independent clones as described in Fig. 4.

(Mo1 and Mo2, two different subclones). As expected, sensitivity for DXR was up-regulated by *mdr1a/1b*-specific RNAi in Colon 26 cells.

Next, we determined how attenuation of *mdr1a/1b* expression in Colon 26 cells affects cell growth. Doubling time for cell division suggested that rate of proliferation of *mdr1a/1b* knockdown Colon 26 cells (KD1 and KD2) was slower than that of control Colon 26 cells (NS1, NS2, Mo1 and Mo2) (Fig. 5A). BrdU staining showed that the number of positively stained cells was lower in case of *mdr1a/1b* knockdown Colon 26 cells compared to control cells (Fig. 5B). Cell cycle analysis showed that cells in Go phase were most abundantly observed in *mdr1a/1b* knockdown Colon 26 cells compared with control Colon 26 cells and cells in the S phase were fewest in case of *mdr1a/1b* knockdown Colon 26 cells compared with control Colon 26 cells (Fig. 5C). Taken together, these results indicate that the growth retardation observed in *mdr1a/1b* knockdown Colon 26 cells was caused by delay of cell cycle based on diminished DNA synthesis.

Suppression of In Vivo Tumourigenesis of Colon 26 Cells through Reduction of mdr1a/1b Function—*In vitro* analysis of cell growth demonstrated that *mdr1a/1b* is closely involved in cell proliferation. However, *in vitro* culture conditions may lack various molecular cues in tumour cell growth in cells with reduced *mdr1a/1b* mRNA. Therefore, finally, we investigated whether *in vivo* tumour development is also affected by reduction of *mdr1a/1b* in Colon 26 cells. Upon subcutaneous inoculation of Colon 26 cells transduced with *mdr1a/1b* specific shRNA or a non-specific control shRNA, tumour weight was significantly reduced in *mdr1a/1b* knockdown Colon 26 cells compared to that in control Colon 26 cells (Fig. 6). Therefore, we concluded that *mdr1a/1b* which has been thought as a drug-resistant molecule in intestinal tumour cells has a functional role in regulation of cell proliferation.

DISCUSSION

Recently, several reports indicated that MDR1 function in tumour cells is associated not only with drug resistance but also tumour cell kinetics. For example, a tumour suppressor protein p53 represses transcription

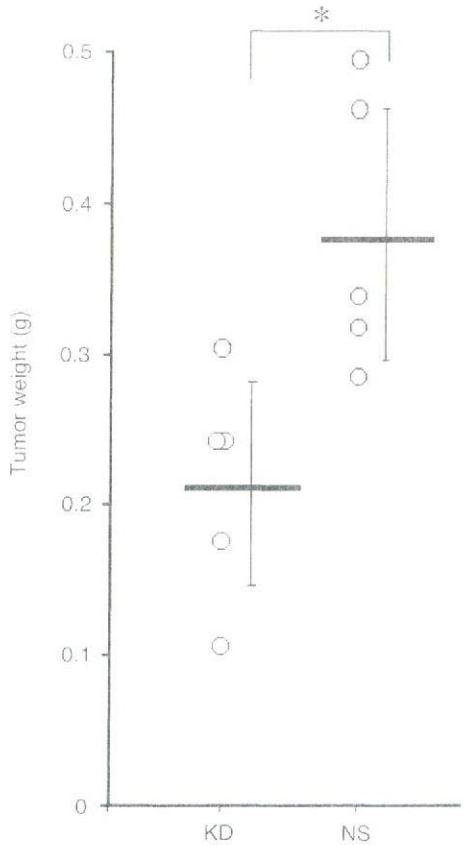

Fig. 6. **Knockdown of *mdr1a/1b* in Colon 26 cells inhibits tumour growth.** *mdr1a/1b* knockdown Colon 26 cells using *mdr1a/1b* specific shRNA (KD) or control Colon 26 cell transduced with a non-specific insert (NS) were inoculated into mice. Fourteen days later, the tumours were dissected and tumour weight was determined. Data shows representative result from three independent experiments; the two groups were statistically significantly different ($P<0.05$).

of *MDR1* gene (*21–23*). MDR1 expression and up-regulation of its activity has been observed in various cells stimulated by growth factors such as EGF (*24*), IGF-I (*25*) and FGF6 (*26*). Moreover, early responsive genes, Fos/jun (AP-1) activated by such growth factors have been suggested to directly regulate *mdr1* expression (*27*). Taken together, these data strongly support the notion that Mdr1 is involved in the cell growth. However, at far as we could determine, attenuation of Mdr1 expression on Colon 26 cells did not affect MAPK activation in the culture condition we used (Fig. 5D). At present, although the mechanism whereby Mdr1 regulates cell proliferation is not clear, association with cell cycle check points, longevity of cells (failure of apoptotic mechanisms) and repair of damaged cellular targets are possible ways in which it can exert this effect. Further precise analysis of MDR1 involvement in the cell cycle of tumour cells is required.

In the present study, we evaluated the function of *mdr1a/1b* in tumour cell proliferation. Our strategy using shRNA that specifically recognized *mdr1a/1b*, knockdown of *mdr1a/1b* was not complete. If mdr1a/1b expression was completely attenuated, it may be possible to achieve more severe suppression of tumour growth. However, as shown in Fig. 1, another member of Mdr family, *mrp1* is expressed in tumour cells. MRP1 has been reported to be expressed in many cancers at high levels (*28*). Although MRP1 may contribute to the baseline drug resistance of cells including normal cells and tumour cells, the specific role of MRP1 in tumour cells remains to be demonstrated. However, if MRP1 has a potential association with cell proliferation as observed in *mdr1a/1b*, inhibition of both *mdr1a/1b* and *mrp1* may effectively inhibit tumour growth.

Taking into account the nature of MDR1 function for drug resistance in tumour cells, the design of non-toxic agents that would overcome MDR in tumour has been considered. However, because of their predicted toxicity, none of the drugs that inhibit MDR1 function are available in the clinic. To overcome this issue, less toxic agents should be developed. One such approach is gene therapy targeting the expression of MDR1 in tumours specifically. Our present data as well as other reports (*29*, *30*) showed that RNAi method could bring about a reduction in the expression and function of MDR1. If a suitable gene therapy system for delivery of RNAi into tumour site is developed, RNAi methods using *mdr1* gene as a target is a likely candidate to inhibit tumour growth.

We thank N. Fujimoto for preparation of plasmid DNA and K. Fukuhara for administrative assistance. This work was partly supported by a Grant-in-Aid from The Ministry of Education, Culture, Sports, Science and Technology of Japan. There is no conflict of interest.

REFERENCES

1. Gottesman, M.M., Fojo, T., and Bates, S.E. (2002) Multidrug resistance in cancer: role of ATP-dependent transporters. *Nat. Rev. Cancer* **2**, 48–58
2. Juliano, R.L. and Ling, V. (1976) A surface glycoprotein modulating drug permeability in Chinese hamster ovary cell mutants. *Biochim. Biophys. Acta* **455**, 152–162
3. Leonard, G.D., Polgar, O., and Bates, S.E. (2002) ABC transporters and inhibitors: new targets, new agents. *Curr. Opin. Investig. Drugs* **3**, 1652–1659
4. Borowski, E., Bontemps-Gracz, M.M., and Piwkowska, A. (2005) Strategies for overcoming ABC-transporters-mediated multidrug resistance (MDR) of tumor cells. *Acta Biochim. Pol.* **52**, 609–627
5. Ambudkar, S.V., Kimchi-Sarfaty, C., Sauna, Z.E., and Gottesman, M.M. (2003) P-glycoprotein: from genomics to mechanism. *Oncogene* **22**, 7468–7485
6. Cordon-Cardo, C., O'Brien, J.P., Boccia, J., Casals, D., Bertino, J.R., and Melamed, M.R. (1990) Expression of the multidrug resistance gene product (P-glycoprotein) in human normal and tumor tissues. *J. Histochem. Cytochem.* **38**, 1277–1287
7. Cordon-Cardo, C., O'Brien, J.P., Casals, D., Rittman-Grauer, L., Biedler, J.L., Melamed, M.R., and Bertino, J.R. (1989) Multidrug-resistance gene (P-glycoprotein) is expressed by endothelial cells at blood-brain barrier sites. *Proc. Natl Acad. Sci. USA* **86**, 695–698
8. Fojo, A.T., Ueda, K., Slamon, D.J., Poplack, D.G., Gottesman, M.M., and Pastan, I. (1987) Expression of a multidrug-resistance gene in human tumors and tissues. *Proc. Natl Acad. Sci. USA* **84**, 265–269

9. Gerlach, J.H., Endicott, J.A., Juranka, P.F., Henderson, G., Sarangi, F., Deuchars, K.L., and Ling, V. (1986) Homology between P-glycoprotein and a bacterial haemolysin transport protein suggests a model for multidrug resistance. *Nature* **324**, 485–489
10. Chen, C.J., Chin, J.E., Ueda, K., Clark, D.P., Pastan, I., Gottesman, M.M., and Roninson, I.B. (1986) Internal duplication and homology with bacterial transport proteins in the mdr1 (P-glycoprotein) gene from multidrug-resistant human cells. *Cell* **47**, 381–389
11. Gros, P., Croop, J., and Housman, D. (1986) Mammalian multidrug resistance gene: complete cDNA sequence indicates strong homology to bacterial transport proteins. *Cell* **47**, 371–380
12. Hsu, I., Lothstein, L., and Horwitz, S.B. (1989) Differential overexpression of three mdr gene family members in multidrug-resistant J774.2 mouse cells. Evidence that distinct P-glycoprotein precursors are encoded by unique mdr genes. *J. Biol. Chem.* **264**, 12053–12062
13. Devault, A. and Gros, P. (1990) Two members of the mouse mdr gene family confer multidrug resistance with overlapping but distinct drug specificities. *Mol. Cell. Biol.* **10**, 1652–1663
14. Schinkel, A.H., Smit, J.J., van Tellingen, O., Beijnen, J.H., Wagenaar, E., van Deemter, L., Mol, C.A., van der Valk, M.A., Robanus-Maandag, E.C., te Riele, H.P., Berns, A.J.M., and Borst, P. (1994) Disruption of the mouse mdr1a P-glycoprotein gene leads to a deficiency in the blood-brain barrier and to increased sensitivity to drugs. *Cell* **77**, 491–502
15. Schinkel, A.H., Mayer, U., Wagenaar, E., Mol, C.A., van Deemter, L., Smit, J.J., van der Valk, M.A., Voordouw, A.C., Spits, H., van Tellingen, O., Zijlmans, J.M., Fibbe, Q.E., and Borst, P. (1997) Normal viability and altered pharmacokinetics in mice lacking mdr1-type (drug-transporting) P-glycoproteins. *Proc. Natl Acad. Sci. USA* **94**, 4028–4033
16. Jonker, J.W., Buitelaar, M., Wagenaar, E., Van Der Valk, M.A., Scheffer, G.L., Scheper, R.J., Plosch, T., Kuipers, F., Elferink, R.P., Rosing, H., Beijnen, J.H., and Schinkel, A.H. (2002) The breast cancer resistance protein protects against a major chlorophyll-derived dietary phototoxin and protoporphyria. *Proc. Natl Acad. Sci. USA* **99**, 15649–15654
17. Yamada, T., Mori, Y., Hayashi, R., Takada, M., Ino, Y., Naishiro, Y., Kondo, T., and Hirohashi, S. (2003) Suppression of intestinal polyposis in Mdr1-deficient ApcMin/+ mice. *Cancer Res.* **63**, 895–901
18. Todaro, G.J. and Green, H. (1963) Quantitative studies of the growth of mouse embryo cells in culture and their development into established lines. *J. Cell Biol.* **17**, 299–313
19. Okamoto, R., Ueno, M., Yamada, Y., Takahashi, N., Sano, H., Suda, T., and Takakura, N. (2005) Hematopoietic cells regulate the angiogenic switch during tumorigenesis. *Blood* **105**, 2757–2763
20. Takakura, N., Watanabe, T., Suenobu, S., Yamada, Y., Noda, T., Ito, Y., Satake, M., and Suda, T. (2000) A role for hematopoietic stem cells in promoting angiogenesis. *Cell* **102**, 199–209
21. Chin, K.V., Ueda, K., Pastan, I., and Gottesman, M.M. (1992) Modulation of activity of the promoter of the human MDR1 gene by Ras and p53. *Science* **255**, 459–462
22. Zastawny, R.L., Salvino, R., Chen, J., Benchimol, S., and Ling, V. (1993) The core promoter region of the P-glycoprotein gene is sufficient to confer differential responsiveness to wild-type and mutant p53. *Oncogene* **8**, 1529–1535
23. Thottassery, J.V., Zambetti, G.P., Arimori, K., Schuetz, E.G., and Schuetz, J.D. (1997) p53-dependent regulation of MDR1 gene expression causes selective resistance to chemotherapeutic agents. *Proc. Natl Acad. Sci. USA* **94**, 11037–11042
24. Yang, J.M., Sullivan, G.F., and Hait, W.N. (1997) Regulation of the function of P-glycoprotein by epidermal growth factor through phospholipase C. *Biochem. Pharmacol.* **53**, 1597–1604
25. Guo, Y.S., Jin, G.F., Houston, C.W., Thompson, J.C., and Townsend, C.M. Jr. (1998) Insulin-like growth factor-I promotes multidrug resistance in MCLM colon cancer cells. *J. Cell. Physiol.* **175**, 141–148
26. Israeli, D., Benchaouir, R., Ziaei, S., Rameau, P., Gruszczynski, C., Peltekian, E., Danos, O., and Garcir, L. (2004) FGF6 mediated expansion of a resident subset of cells with SP phenotype in the C2C12 myogenic line. *J. Cell Physiol.* **201**, 409–419
27. Osborn, M.T. and Chambers, T.C. (1996) Role of the stress-activated/c-Jun NH2-terminal protein kinase pathway in the cellular response to adriamycin and other chemotherapeutic drugs. *J. Biol. Chem.* **271**, 30950–30955
28. Nooter, K., Westerman, A.M., Flens, M.J., Zaman, G.J., Scheper, R.J., van Wingerden, K.E., Burger, H., Oostrum, R., Boersma, T., Sonneveld, P., Gratama, J.W., Kok, T., Eggermont, A.M.M., Bostman, F.T., and Stoter, G. (1995) Expression of the multidrug resistance-associated protein (MRP) gene in human cancers. *Clin. Cancer Res.* **1**, 1301–1310
29. Duan, Z., Brakora, K.A., and Seiden, M.V. (2004) Inhibition of ABCB1 (MDR1) and ABCB4 (MDR3) expression by small interfering RNA and reversal of paclitaxel resistance in human ovarian cancer cells. *Mol. Cancer Ther.* **3**, 833–838
30. Pichler, A., Zelcer, N., Prior, J.L., Kuil, A.J., and Piwnica-Worms, D. (2005) In vivo RNA interference-mediated ablation of MDR1 P-glycoprotein. *Clin. Cancer Res.* **11**, 4487–4494

Hearing Research 245 (2008) 73–81

Contents lists available at ScienceDirect

Hearing Research

journal homepage: www.elsevier.com/locate/heares

Research paper

Involvement of platelet-derived growth factor receptor-β in maintenance of mesenchyme and sensory epithelium of the neonatal mouse inner ear

Hisamitsu Hayashi [a,*], Takahiro Kunisada [b], Nobuyuki Takakura [c], Mitsuhiro Aoki [a], Keisuke Mizuta [a], Yatsuji Ito [a]

[a] Department of Otolaryngology, Graduate School of Medicine, Gifu University, 1-1 Yanagido, Gifu-shi, Gifu 501-1194, Japan
[b] Department of Tissue and Organ Development, Gifu University Graduate School of Medicine, 1-1 Yanagido, Gifu-shi, Gifu 501-1194, Japan
[c] Department of Signal Transduction, Research Institute for Microbial Diseases, Osaka University, 3-1 Yamada-oka, Suita-shi, Osaka 565-087, Japan

ARTICLE INFO

Article history:
Received 10 March 2008
Received in revised form 27 August 2008
Accepted 29 August 2008
Available online 12 September 2008

Keywords:
Platelet-derived growth factor receptor
Inner ear
Mesenchymal tissue
Neonatal mouse
Immunohistochemistry
APB5

ABSTRACT

Platelet-derived growth factor receptor (PDGFR) signaling has been demonstrated to play a pivotal role in early embryonic development. Although the expression of PDGF in the inner ear has been studied by RT–PCR, how PDGFR is involved there remains largely unclear. In the current study, we used the antagonistic anti-PDGFR-β antibody, APB5, to investigate the role of PDGFR-β in the neonatal mouse inner ear. PDGFR-β was detected immunohistochemically in the mesenchymal tissue adjacent to the sensory epithelium of the inner ear, and a ligand for PDGFR-β was detected around the sensory epithelium. To determine whether this expression plays a functional role, we injected APB5 into neonates to block the function of PDGFR-β. Mesenchymal tissue defects and abnormal capillaries with irregular shapes, especially in the cochlear lateral wall, were detected in APB5-treated mice. The results of a TUNEL assay revealed that not only the adjacent mesenchymal cells but also the sensory epithelial cells underwent cell death. These results indicate that PDGFR-β signals are required for the survival of the capillary and mesenchymal cells in the neonatal mouse inner ear and also indirectly implicate these signals in the survival of the sensory epithelium.

1. Introduction

The platelet-derived growth factor (PDGF) family of ligands, originally isolated because of their ability to promote the proliferation of mesenchymal cells (Heldin et al., 1985), is known to have critical roles in cellular differentiation and to be essential during animal development (Hoch and Soriano, 2003). The PDGF signaling network consists of four ligands, i.e. PDGF-A, PDGF-B (Heldin et al., 1998), PDGF-C (Li et al., 2000), and PDGF-D (LaRochelle et al., 2001; Bergsten et al., 2001), and two receptors, PDGF receptor (PDGFR)-α and PDGFR-β. All PDGFs function as disulfide-linked homodimers, but only PDGF-A and -B can form functional heterodimers. Each of these PDGF chains has a different receptor affinity. Although, PDGFR-α is bound and activated by all of the dimeric forms of PDGF-A, -B, or -C, PDGFR-β is activated exclusively by PDGF-BB and PDGF-DD homodimers. The polyfunctional effect of PDGFs on various cells suggests their roles in multiple processes such as cell proliferation, survival, and chemotaxis, as well as wound healing (Davidson et al., 1999), gastrulation (Ramachandran et al., 1997), glial cell development (Fruttiger et al., 1999), angiogenesis (Risau et al., 1992), and atherosclerosis (Sano et al., 2001). Gene-targeting experiments have led to the creation of knockout mice deficient in PDGFR-α (Soriano, 1997) or PDGFR-β (Soriano, 1994). Phenotypically, PDGFR-α mutants exhibit multiple defects including reduced growth, dilation of the pericardium, subepidermal blebs, a wavy neural tube, and defects in the yolk sac. The PDGFR-β mutants are hemorrhagic, thrombocytopenic, and severely anemic. Either type of mutant dies at the embryonic stage, or PDGFR signaling has been thought to play a pivotal role in early embryonic development.

A few reports are available on the expression of PDGF in the inner ear. PDGFR-α mRNA is detected in the sensory epithelium of the rat utricle by RT–PCR (Saffer et al., 1996). The presence of mRNA for a wide variety of growth factors and growth factor receptors including PDGFR has been identified in the postnatal rat cochlea (Malgrange et al., 1998). RT–PCR analysis also reveals that PDGFs and their receptors exist in the developing and adult rat cochlea (Lee et al., 2004). Furthermore, the influence of PDGF on the sensory epithelium of the inner ear has been investigated

Abbreviations: PDGFR, platelet-derived growth factor receptor; TUNEL, terminal deoxynucleotidyl transferase biotin-dUTP nick end labeling

* Corresponding author. Tel.: +81 58 230 6279; fax: +81 58 230 6280.
E-mail addresses: hh@gifu-u.ac.jp (H. Hayashi), kunisad@gifu-u.ac.jp (T. Kunisada), ntakaku@biken.osaka-u.ac.jp (N. Takakura), aoki@gifu-u.ac.jp (M. Aoki), kmizuta@gifu-u.ac.jp (K. Mizuta), ity@gifu-u.ac.jp (Y. Ito).

0378-5955/$ - see front matter © 2008 Elsevier B.V. All rights reserved.
doi:10.1016/j.heares.2008.08.011

in vitro. Zheng et al. (1997) used partially dissociated sheets of early postnatal rat utricular epithelium to screen a large number of different growth factors for their ability to initiate a cell proliferation response, and PDGF did not have any detectable mitogenic effect on the utricular epithelial cells. Outer hair cell losses in the adult guinea pig organ of Corti cultures can also be prevented by treatment with several of the growth factors tested, but PDGF had no significant effect on outer hair cell survival in explants of adult organ of Corti (Malgrange et al., 2002). Accordingly, although the expression of PDGF isoforms and PDGFRs in the inner ear has been studied by RT-PCR, they might have no appreciable effect on the survival or proliferation of the sensory epithelia *in vitro*; and thus, how PDGFR is involved in the inner ear remains largely unclear. The aim of the present study was to elucidate the possible roles of PDGF signaling in the inner ear. Whereas, gene-targeting studies in mice indicate that PDGF-A and PDGFR-β are critical in the embryonic stage, the search for the role of PDGF signaling has been elusive during late embryonic and postnatal stage because of their embryonic lethality. During late embryonic and early postnatal stages, hair cells start to mature by growing stereociliary bundles (Xiang et al., 1998). During this period, we tried to create PDGFR-β loss-of-function in the mouse to clarify the roles of PDGFR-β in the inner ear. For this purpose, we introduced the strategy of administering antagonistic rat monoclonal anti-murine PDGFR-β antibodies, APB5, with high specificity for PDGFR-β, to neonatal mice to dissect the signal transduction pathways coming from PDGFR-β. The blocking effect of APB5 on PDGFR-β has been shown earlier: the addition of APB5 to cultures of murine bone marrow cells suppressed the proliferation of hematopoietic progenitors and immunoblot analysis with APB5 showed that phosphorylation of PDGFR-β in a line of vascular smooth muscle cells was completely inhibited (Sano et al., 2001). Sano and colleagues also reported that blockade of the PDGFR-β pathway by administration of APB5 to newborn mice caused deformation of the glomerular structure in the kidneys (Sano et al., 2002). This phenotype is morphologically similar to that of PDGF-B and PDGFR-β mutant mice during the embryonic stage, both of which show markedly abnormal glomerular development (Soriano, 1994).

First, we examined the localization of PDGFR-β in the inner ear of neonatal mice by immunohistochemistry with APB5. We then investigated the phenotype of the inner ear after daily administration of APB5 to neonatal mice. These results indicate that PDGFR-β signals are required for survival of the capillaries and mesenchymal cells in the neonatal mouse inner ear and are also indirectly implicated in the survival of the sensory epithelium.

2. Materials and methods

2.1. Animals

Pregnant ICR female mice were purchased from Japan SLC Incorporated (Shizuoka, Japan). The mice were kept in a temperature-controlled facility on a 14-h light/10-h dark cycle with free access to food and water. Animal care was under the supervision of the Division of Animal Experiment, Life Science Research Center, Gifu University. All experimental protocols in this study were approved by the Animal Care and Use Committee of Gifu University.

2.2. Administration of rat monoclonal antibody (APB5) to mice

Earlier, we described the preparation of APB5, a rat monoclonal anti-murine PDGFR-β antibody, and its antagonistic effects on the PDGFR-β signal transduction pathway *in vivo* and *in vitro* (Sano et al., 2001). The hybridoma line secreting antibodies against PDGFR-β was grown in athymic nude mice, and monoclonal antibodies were purified from ascitic fluid by ammonium sulfate precipitation and gel filtration using Sephadex™ G-25 medium (GE Healthcare). The antibody APB5 was dissolved in a volume of PBS sufficient to result in a final antibody concentration of 15 mg/ml, determined by measuring the absorbance at OD_{280}. To evaluate the purity of the antibody APB5, molecular weight was detected by staining with Coomassie Brilliant Blue after sodium dodecyl sulfate-polyacrylamide gel electrophoresis. APB5 is also available on a commercial basis (eBioscience).

The day of birth of the newborn mice was defined as postnatal day 0 (P0), and the mice were injected intraperitoneally every day with either 100 μg of APB5 in PBS or the equivalent volume of PBS as the control. The dose usage of APB5 was based on the animal weight and deduced from the procedure of Sano et al. (2001,2002). Some mice were euthanized at P5 and others at P9.

At the start of the study, 10 mice were to be euthanized at P5 (APB5-injected ones: $n = 5$; controls: $n = 5$), and 31 mice were to be euthanized at P9. Experimental animals in the latter case were divided into four groups according to the period of administration. Group 1 mice ($n = 7$) were administered APB5 from P0 to P4, Group 2 mice ($n = 7$) from P4 to P8, Group 3 mice ($n = 12$) from P0 to P8, and control ($n = 5$) from P0 to P8.

2.3. Histochemistry

Briefly, each mouse was decapitated; and its head was fixed in 4% paraformaldehyde for one day at 4 °C, followed by decalcification in 5% EDTA in PBS, pH 7.4, for three days at 4 °C. After PBS rinses, the samples were immersed in 20% sucrose in PBS for at least 12 h at 4 °C and then snap-frozen in O.C.T. compound (Sakura Finetek). The samples were stored at −80 °C until used, and then were sectioned at a thickness of 8 μm in a cryostat. For hematoxylin and eosin (H&E) staining, the sections were stained with H&E solution (Wako Pure Chemical Industries).

2.4. Immunoperoxidase

Frozen sections were processed using a Universal LSAB™ 2 Kit (Dako), based on the labeled streptavidin–biotin (LSAB) method. Endogenous peroxidase activity was blocked with 0.5% H_2O_2 in methanol for 10 min. The sections were then incubated overnight at 4 °C with APB5 (20 mg/ml) in PBS containing 1% bovine serum albumin (BSA). After two washes of the sections in PBS, they were reacted with biotinylated rabbit anti-rat immunoglobulin (Dako) for 15 min and then with streptavidin-peroxidase conjugate for another 15 min. The enzymatic reaction was detected using a freshly prepared Dako liquid DAB (3,3-diaminobenzidine tetrahydrochloride) substrate-chromogen solution for 10 min. The sections were then counterstained with hematoxylin. For the negative control, the primary antibody was replaced by PBS in the staining method. Specimens were observed with an Olympus microscope (Tokyo, Japan) equipped with the proper filters.

2.5. Double-labeling immunofluorescence

The sections were rinsed in PBS and incubated in PBS containing 2% BSA and 1% normal goat serum for 30 min to minimize non-specific binding, and subsequently incubated overnight at 4 °C with the first primary antibody (1 mg/ml), which recognizes PDGF-B (sc-7878, Santa Cruz Biotech.), the ligand of PDGFR-β (Basciani et al., 2004). To ensure specificity, control tests included the following: replacement of the anti-PDGF-B antibody with PBS completely abolished immunolabeling, and by immunohistochemistry using this primary antibody, PDGF-B was expressed in many capillaries in the brain of an E17 embryo (Lindahl et al., 1997a). An Alexa Fluor 555-conjugated anti-rabbit immunoglobulin (molecular probes)

was used at a concentration of 20 mg/ml for 30 min as the secondary antibody. Following extensive washing in PBS, the sections were incubated overnight at 4 °C with APB5 (20 mg/ml) and after rinsing, an Alexa Fluor 488-conjugated anti-rat immunoglobulin (molecular probes) was used at a concentration of 20 mg/ml for 30 min. The sections were rinsed in PBS, mounted in a mixture of PBS and glycerol (1:9), and then observed with a Zeiss LSM510 confocal microscope. Alexa Fluor 488 was excited using a 488-nm argon ion laser and Alexa Fluor 555 using a 543-nm He/Ne laser.

2.6. Terminal deoxynucleotidyl transferase nick end labeling (TUNEL) assay

To identify nuclei in which DNA strand breaks had occurred, we applied the TUNEL procedure to sections from APB5-treated mice ($n = 5$) and control ones ($n = 5$), and counted the cells present in five sections per APB5-treated animal and control, respectively, using an ApopTag Fluorescein *in situ* Apoptosis Detection Kit (Chemicon), according to the specifications and instructions recommended by the manufacturer. In brief, after having been washed with PBS for 15 min, the sections were soaked in the equilibration buffer of the kit for 10 min at room temperature and then incubated at 37 °C for 60 min in a moist chamber with the working buffer containing terminal deoxynucleotidyl transferase (TdT), digoxigenin-11-dUTP, and dATP. The reaction was terminated by transferring the sections to prewarmed stop/wash buffer for 30 min at 37 °C. The sections were covered with fluorescein isothiocyanate (FITC)-conjugated anti-digoxigenin antibody and incubated for 30 min at room temperature.

The cochleas were serially sectioned (8 μm) parallel to the midmodiolus plane, and five sections were randomly selected with more than one section between two of them discarded to avoid counting the same nuclei in both sections. The sections were double-stained with the Hoechst33342 (Sigma) counterstain and TUNEL reagents. The ratio of TUNEL-positive cells to total cells in the organ of Corti was calculated, and the average of the five sections was determined. For the saccule and utricle, five sections including the sensory epithelium were randomly selected, as done for the cochlea. TUNEL-positive cells and total cells were counted in a 100-μm length of the sensory epithelium of each section. The ratio was calculated, and the average of the five sections was subjected to statistical analysis.

2.7. Statistical analysis

Cell death data were expressed as means and standard deviations, and were analyzed by Student's *t*-test. A *p-value* <0.05 was considered statistically significant.

3. Results

3.1. Expression of PDGFR-β in the inner ear mesenchymal tissue of neonatal mice

At postnatal day 3 (P3), PDGFR-β immunostaining was observed in the mesenchymal tissue subjacent to the sensory epithelium of the saccule (Fig. 1D) and the utricle (Fig. 1F), but not in the sensory epithelium including the hair cells and supporting cells. As shown in Fig. 1A, extensive PDGFR-β expression was observed in the tissue beneath the basement membrane of the organ of Corti, in the spiral limbus and spiral ligament, but was almost undetectable in the organ of Corti. Also, capillary pericytes in the lateral wall of the cochlea, including the stria vascularis, showed strong immunoreactivity for PDGFR-β (Fig. 1B). The negative controls, with the primary antibody APB5 omitted, did not show positive immunostaining in the tissue sections (Fig. 1C, E and G).

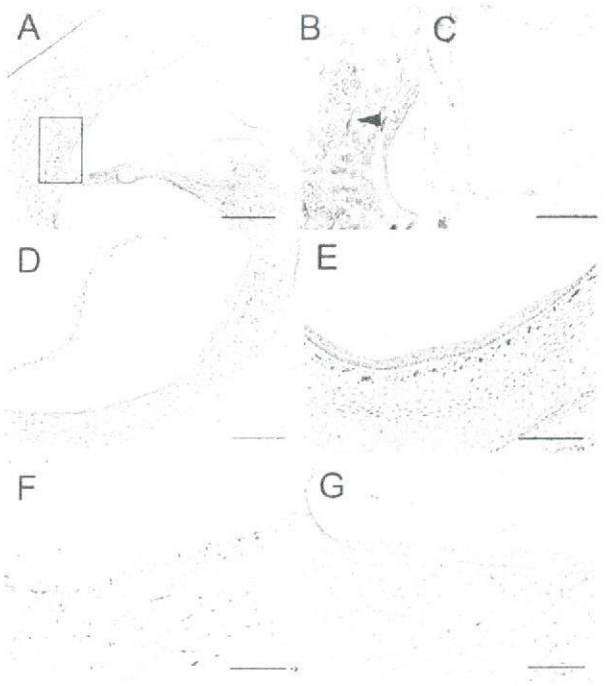

Fig. 1. Expression of PDGFR-β in the postnatal mouse inner ear. Immunohistochemistry with APB5 was performed on transverse sections of the inner ear from ICR mice at postnatal day 3 (P3). PDGFR-β expression was visualized as a brown reaction product. (A) PDGFR-β was expressed in the lateral wall of the cochlea and the mesenchymal tissues adjacent to the sensory epithelium, and rather specifically in tissues surrounding the capillaries (B, arrowhead). In the saccule (D) and utricle (F), PDGFR-β was also expressed in mesenchymal tissues under the sensory epithelium. Control sections of the cochlea (C), saccule (E) and utricle (G) were incubated without the primary antibody, APB5. Note that non-specific reactions were evident in hematopoietic cells in both APB5-treated and control specimens but that the positive staining in mesenchymal tissues was detected only in the APB5-treated specimens. Scale bar, 100 μm.

3.2. Contiguous pattern of expression of PDGFR-β and its ligand in the neonatal inner ear

To localize the receptor and ligand in the neonatal inner ear, we performed double-immunofluorescence with APB5 and the antibody to PDGF-B, one of the ligands for PDGFR-β. In transverse sections immunostained with both anti-PDGF-B antibody and APB5, the expression of the ligand around the sensory epithelium was nearly contiguous with that of PDGFR-β in mesenchymal tissues adjacent to the sensory epithelium (Fig. 2C, I and L). The expression of PDGFR-β surrounding the spiral vessel and of the ligand inside the spiral vessel was also reciprocal (Fig. 2A and F). Staining with APB5, though weaker than that in the region subjacent to the organ of Corti and surrounding the spiral vessel, was present in the supranuclear regions of hair cells. Immunofluorescence staining in the tectorial membrane was non-specific, because the double-stained area with PDGF-B and PDGFR-β on the tectorial membrane was present (Fig. 2F) but not in Fig. 1A.

3.3. Impaired mesenchymal tissues and abnormal capillaries adjacent to sensory epithelium in neonatal mice injected with APB5

To investigate the possible involvement of PDGFR-β signal transduction in the inner ear *in vivo*, we injected APB5 to block receptor function. Because of the pleiotropic action of PDGF, inhibition of PDGFR-β function during the neonatal period resulted in high lethality. In fact, mice treated with APB5 for more than 10

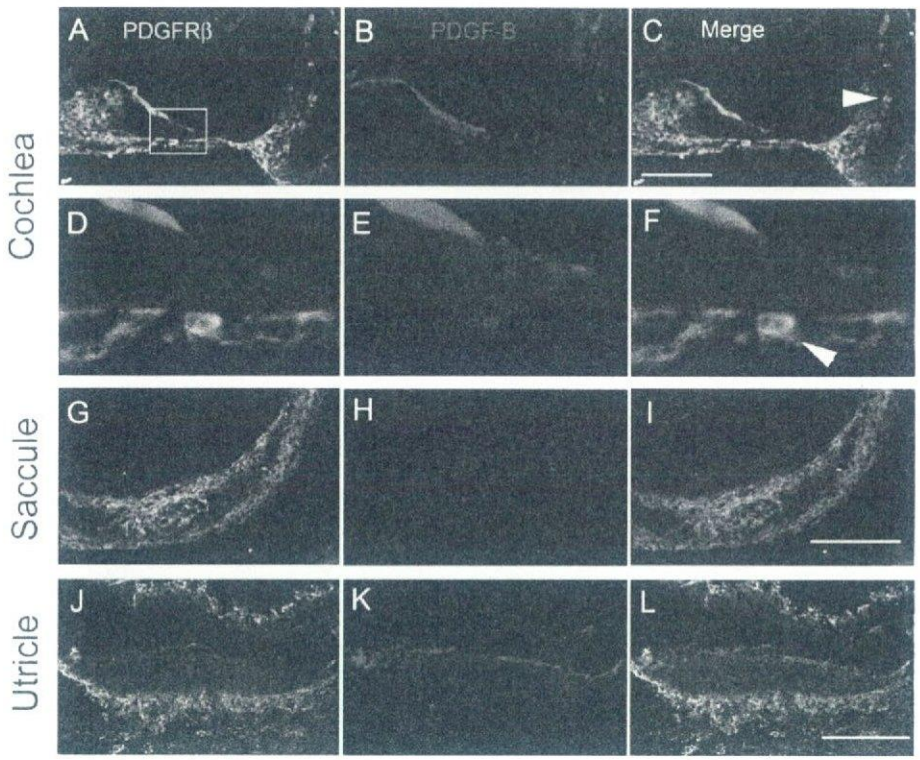

Fig. 2. Contiguous expression of PDGF-B and PDGFR-β in the P3 mouse inner ear. (A–L). Sections of cochlea (A–F), saccule (G–I), and utricle (J–L) are shown. PDGF-B is one of the ligands for PDGFR-β. Confocal optical sections of the inner ear were stained with antibodies against PDGF-B (red) and PDGFR-β (green). The expression of PDGF-B around sensory epithelia and of PDGFR-β in mesenchymal tissue was almost contiguous, indicative of the local signal activation. The expression of PDGFR-β surrounding the spiral vessel and of the ligand inside the spiral vessel was also reciprocal (white arrowheads) at high magnification of the rectangle in A (C and F). PDGFR-β signal was weakly present in the supranuclear regions of hair cells (D and F). Scale bar, 100 μm.

consecutive days were very likely to die. To keep the mice viable and to avoid the effect of metabolic imbalance due to failure of multiple organs, we selected a short-term injection schedule in which an intraperitoneal injection of APB5 was given from P0 to P4 or P0 to P8 (Table 1).

When the inner ear from mice euthanized at P5 was observed by H&E staining, no difference was found between mice injected with APB5 and those given PBS (data not shown). When APB5-treated mice were euthanized at P9, however, capillaries in the lateral wall of the cochlea had irregular and dilated shapes compared with the control (Fig. 3A–C). More strikingly, tissue defects were present in the lateral wall of the cochlea (Fig. 3A, D and E) and not only in the mesenchymal region of the saccule but also in its sensory epithelium (Fig. 3G and H). These abnormalities were observed from the apex to the base of the cochlea. In the utricle, the defect found in the cochlea and saccule was not detected (data not shown). As shown in Fig. 3F and I, injection with PBS caused no such change in the mice euthanized at P9. An additional experiment for the extended injection schedule was performed to assess the time-dependent APB5 effect on mouse. In Table 1, the number of animals employed and ears observed in this study, and the incidence of defects in the cochlea, saccule, and utricle are summarized.

Table 1
Number of APB5-treated mice (ears)

Experimental group	Number of mice at P0	Survival rate at P9 (%)	Number of mice (ears)	Deficiency (+) at P9	Deficiency (−) at P9
Control	5	100	Cochlea	0 (0)	5 (10)
			Saccule	0 (0)	5 (10)
			Utricle	0 (0)	5 (10)
Group 1: injected from P0 to P4	7	57	Cochlea	3 (6)	1 (2)*
			Saccule	2 (4)	2 (4)*
			Utricle	0 (0)	4 (8)
Group 2: injected from P4 to P8	7	71	Cochlea	2 (4)	3 (6)
			Saccule	2 (4)	3 (6)
			Utricle	0 (0)	5 (10)
Group 3: injected from P0 to P8	12	42	Cochlea	4 (8)	1 (2)*
			Saccule	4 (8)	1 (2)*
			Utricle	0 (0)	5 (10)

Fisher's exact tests were used to determine whether the number of ears affected was significantly different in either group compared with the control group (*$p < 0.05$). Statistical tests were only applied to ears, and not to individual mice.

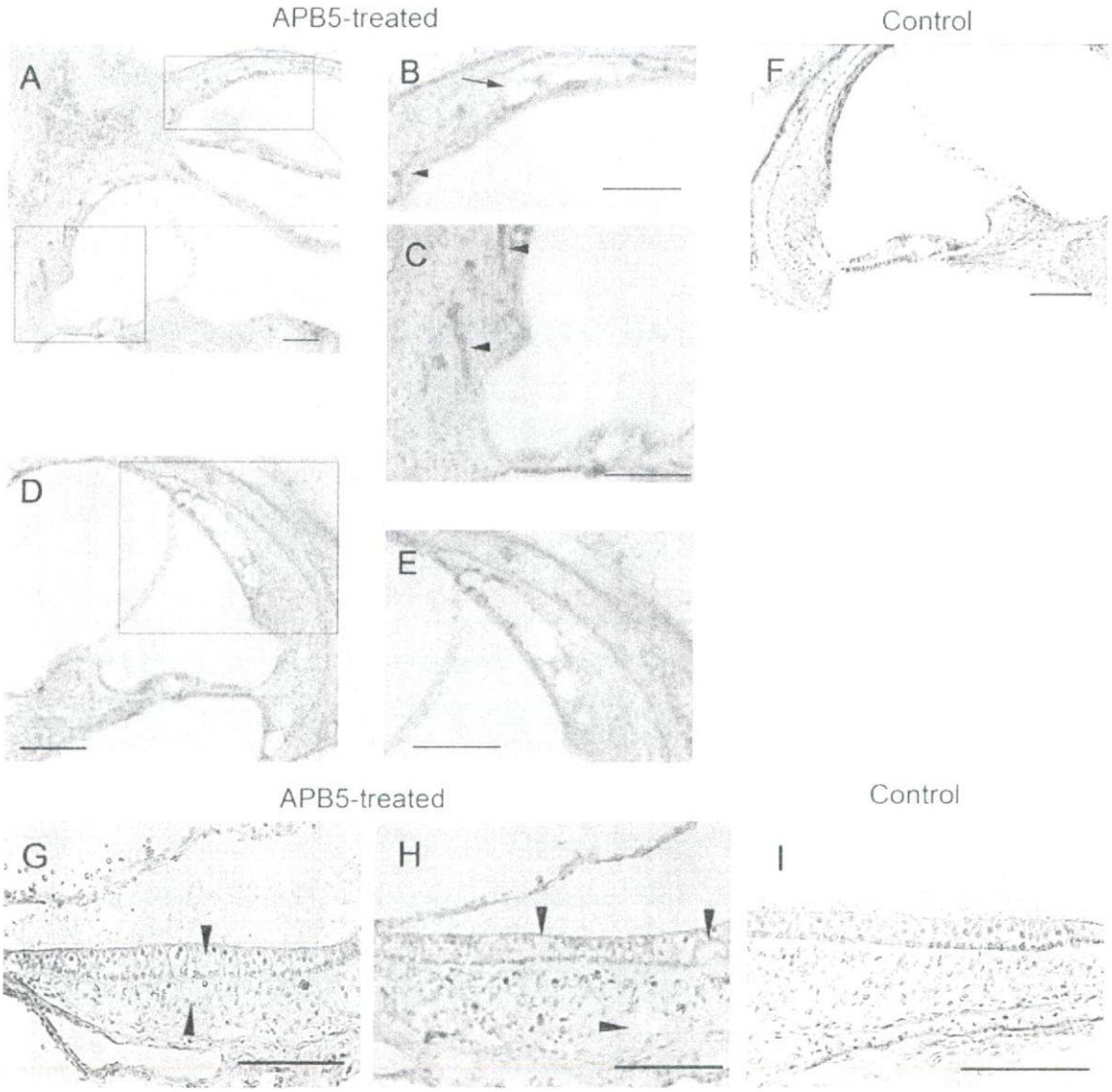

Fig. 3. Histology of the inner ear from the APB5-injected mouse. Transverse sections of the inner ear from control (F and I) and APB5-injected (A–E, G and H) mice at postnatal day 9 (P9) are shown. (B and C) indicate high magnification of the rectangle in (A), and (E) is the high magnification image of the rectangle in (D). (A–E) Not only were abnormal capillaries (arrowheads) present but also mesenchymal defects (arrow) in the lateral wall of the cochlea. Capillaries in the spiral ligament show irregular and dilated shapes compared with the control (B and C, arrowheads). (G and H) Tissue defects (arrowheads) were found in the saccular macula and surrounding mesenchyme. The sensory epithelia of the cochlea seemed to show no deterioration. Scale bar, 100 μm.

Defects were determined based on whether a mesenchymal defect was present in the lateral wall of the cochlea and adjacent to the sensory epithelium of the vestibule. The incidence of the abnormality in the cochlea and saccule of Groups 1 and 3 was significantly higher than that of the control, while histological analysis of the utricle revealed no change in each group compared with the control group. Group 2 mice injected with APB5 for the last five days showed no significant differences in mesenchymal defects of the inner ear compared with the control group.

3.4. Induction of cell death in the sensory epithelium by PDGFR-β blockade

H&E staining revealed that the sensory epithelium of the cochlea and the utricle of APB5-treated mice showed no appreciable change compared with that of the control mice. To study further the effect of APB5 administration on the sensory epithelium of the inner ear, we conducted an *in situ* TUNEL assay, which detects cells at early stages of apoptosis.

The inner ear of APB5-treated mice, especially the cochlea and saccule, presented a much larger number of TUNEL signals than that of the controls. Most of the cells emitting TUNEL-positive signals were located in the spiral ligament, spiral limbus, organ of Corti, saccular macula, and the mesenchymal tissue under the sensory epithelium of the saccule (Fig. 4A and C–E). In contrast, the inner ears of the control mice and also the utricle of APB5-treated mice showed only a few TUNEL signals (Fig. 4B and F).

To quantify the cell death, we estimated the ratio of TUNEL-positive cells to the total number of nuclei in the sensory epithelia. The cell death ratio for the cochlea and saccule from mice injected with APB5 was significantly higher than that for the control mice (Fig. 4G and H), whereas the ratio for the utricle indicated no sig-

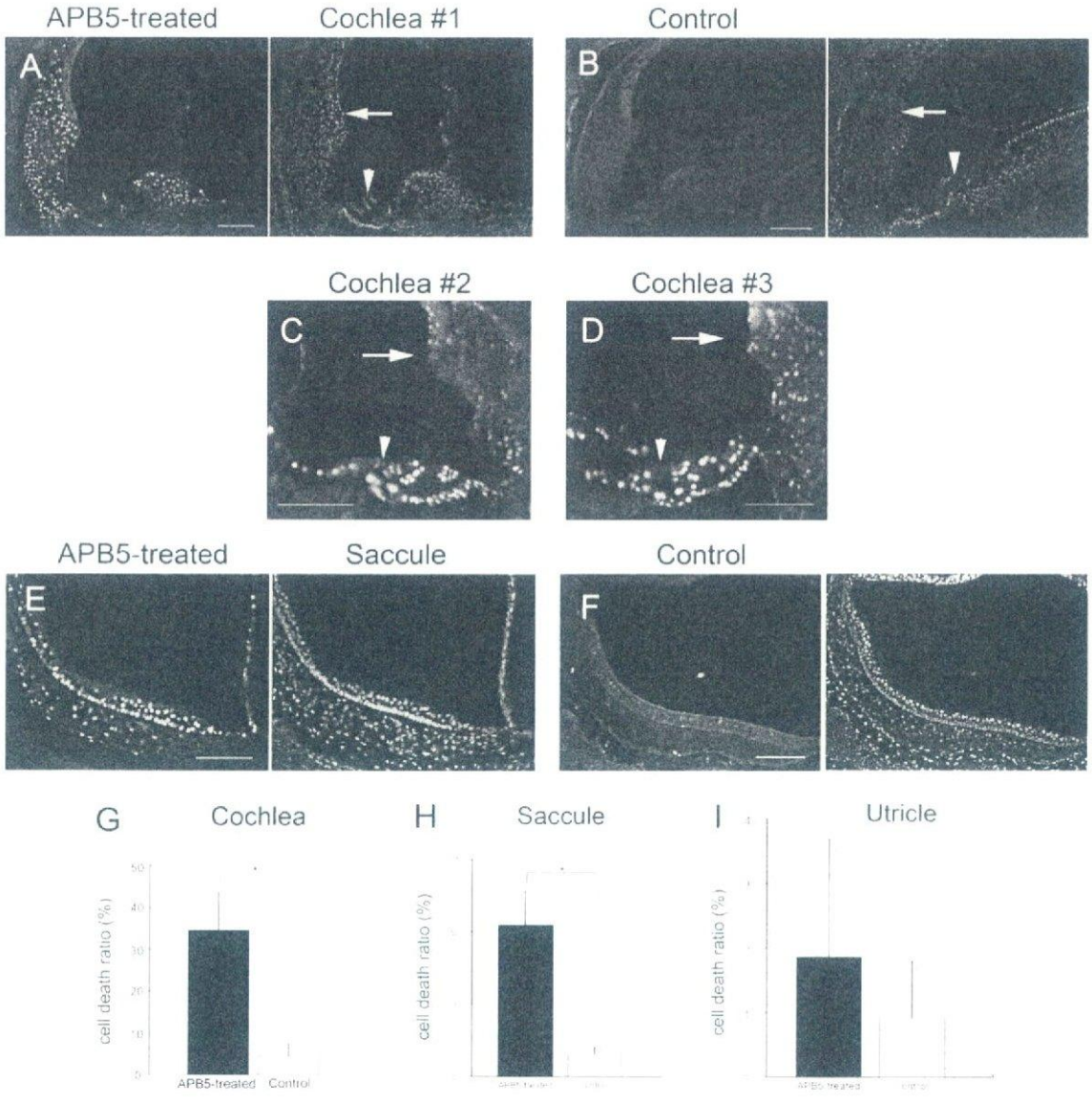

Fig. 4. Micrographs of the cochlea, saccule, and utricle examined by the TUNEL method. Neonatal mice were injected everyday with PBS or APB5 and killed at P10 (A–F). The frozen sections of the inner ear were subjected to TUNEL analysis and nuclear staining of the same field image, as described in Section 2. The cochlea (A), especially the spiral ligament and the spiral limbus, and the saccular macula (E) of APB5-treated mouse presented a larger number of TUNEL signals (green) than did the control cochlea (B) or saccule (F). (A and B) Arrows and arrowheads denote the organ of Corti and the stria vascularis, respectively. (C and D) The other cochleas showed TUNEL signals in the organ of Corti (white arrowheads) and the lateral wall (white arrows). Quantitative analysis of the effect of APB5 on cell death in the sensory epithelium showed that, in the cochlea (G) and saccule (H) of mice treated with APB5 ($n = 5$), the proportion of cell death increased significantly compared with that for the control ($n = 5$; $p < 0.05$), but not in the case of the utricle (I). A statistically significant difference is noted with an asterisk. Scale bar, 100 μm.

nificant difference between the APB5-treated mice and controls. Thus blockade of the PDGFR-β pathway in the neonatal inner ear also induced cell death in the sensory epithelium of the cochlea and saccule.

4. Discussion

In the current study, we investigated the role of PDGFR-β in the inner ear by blocking the PDGFR-β signal in the neonatal mouse with the administration of an antagonistic monoclonal antibody. Neonatal mice injected daily with anti-PDGFR-β antibody showed mesenchymal defects and microvascular abnormalities in the inner ear. The TUNEL assay revealed that not only the mesenchymal cells subjacent to the sensory epithelium of the inner ear but also the sensory epithelial cells of the cochlea and saccule underwent cell death.

We first performed double-labeling immunofluorescence with antibodies against PDGF-B and PDGFR-β on sections of mouse inner ear to examine the localization of each. The expression of the ligand (PDGF-B) around the sensory epithelium and of the receptor (PDGFR-β) on mesenchymal tissue was almost contiguous. The expression of PDGFR-β surrounding the spiral vessel and of the ligand inside the spiral vessel was also reciprocal. A similar expression pattern of PDGF has been observed during organogenesis in mice, i.e. PDGFR-β was expressed rather specifically on mural cells surrounding the blood vessels, and PDGF-B was expressed by sprouting endothelium (Lindahl et al., 1997a). In the process of mesangial cell recruitment in the kidney, the endothelial cells ex-

pressed PDGF-B and mesangial cells expressed PDGFR-β (Lindahl et al., 1998). During organogenesis such as lung, retina, testis, gut, and hair, epithelial cells expressed PDGF-A, whereas, adjacent mesenchymal cells expressed PDGFR-α (Boström et al., 1996; Lindahl et al., 1997b; Fruttiger et al., 1996, 2000; Gnessi et al., 2000; Karlsson et al., 1999, 2000). Although our present study did not address the embryonic stage but rather the postnatal period, our findings are compatible with the comprehensive fact that the ligand of PDGF is expressed on the epithelium and the receptor on the mesenchymal tissue. It is conceivable that the reciprocal interaction involving PDGF-B and PDGFR-β between epithelial and mesenchymal tissues is also at play in the inner ear of the neonatal mouse. On the other hand, PDGFR-β was slightly expressed in the organ of Corti. Although PDGF did not have any detectable mitogenic effect on the utricular epithelial cells *in vitro* (Zheng et al., 1997), PDGFR-β may function as a survival factor in the sensory epithelium of the cochlea *in vivo*.

To test whether antagonistic rat monoclonal anti-murine PDGFR-β antibodies, e.g. APB5, could affect the inner ear in neonatal mice, we studied the inner ear in mice injected with APB5 from postnatal day 0. Whereas, the inner ears of mice administered APB5 for five days showed no apparent phenotype compared with those of control mice, tissue defects and microvascular abnormalities were observed in the cochlear lateral wall and mesenchymal tissue adjacent to the sensory epithelium of mice administered with APB5 for nine days. In the case of mice euthanized at P9 after the administration of APB5, the incidence of abnormalities in the cochlea and saccule of the group injected APB5 from P0 to P4 was significantly higher than that of the control. These experiments with some administration plans revealed that the cochlea and saccule in mouse administered APB5 from birth had a tendency to increase the incidence of the abnormality. We speculate that, within several days after birth, the cochlea and saccule are more sensitive to APB5 and it takes a few days to develop mesenchymal defects after the first administration of APB5.

In the PDGF-B- and PDGFR-β-null mutants, which die at late gestation, multiple cardiovascular abnormalities are apparent from an earlier embryonic age, including cardiac dilation, abnormal kidney glomeruli lacking mesangial cells, an abnormal placenta labyrinthine layer, and dilation of large- and small-caliber blood vessels (Levéen et al., 1994; Soriano, 1994; Lindahl et al., 1997a; Hellström et al., 1999; Ohlsson et al., 1999). In APB5-treated mice, blockade of PDGFR-β signals caused deformation of the glomerular capillary (Sano et al., 2002). As described above, PDGF-B was expressed on vascular endothelial cells and PDGFR-β on mural cells during development. Therefore, a paracrine signaling network is likely to exist in different but closely located cell types in blood vessels (Betsholtz, 2004). Given that reciprocal signaling between vascular endothelial cells and mural cells is blocked, lack of mural cells leads to blood vessel dilation, endothelial cell hyperplasia, and microaneurysm formation as seen in the PDGF-B and PDGFR-β knockouts (Hellström et al., 2001). Similarly, microvascular abnormalities seen in the inner ear of APB5-treated mouse may be related to the fact that reciprocal signaling between endothelial cells and mural cells is blocked by APB5. Another striking finding in this study was the mesenchymal defects, especially in the cochlear lateral wall and the saccule. PDGFR-β was earlier reported to be expressed on connective tissue cells (Heldin and Westermark, 1999). In the current study, PDGFR-β was expressed mainly in the spiral ligament composed of connective tissue cells or fibrocytes, and administration of APB5, an antibody against PDGFR-β, caused mesenchymal defects. This finding suggests that PDGFR-β plays a direct role in survival of mesenchymal tissue including fibrocytes in the lateral wall of the cochlea.

Mesenchymal abnormalities in the cochlear lateral wall of APB5-injected mouse may result in auditory dysfunction, because the cochlear lateral wall, consisting of the stria vascularis and the spiral ligament, plays a significant role in the regulation of electrolyte homeostasis in the inner ear. In fact, a rat model with the mitochondrial toxin, 3-nitropropionic acid, injected into the inner ear revealed a pathological change in the fibrocytes of the lateral wall and spiral limbus and showed acute sensorineural hearing loss (Kamiya et al., 2007). The role of the stria vascularis is to pump Na^+ ions out of the endolymph and maintain its ionic composition. The spiral ligament is composed mainly of connective tissue elements including extracellular material and fibrocytes of mesenchymal origin. Aided by gap junctions and NaK-ATPase pumps, the spiral ligament is thought to pump K^+ out of the perilymph and transport it into the endolymph to maintain the high concentration of K^+ in the latter (Raphael and Altschuler, 2003; Wangemann, 2002). This mesenchymal abnormality induced by APB5 also suggests that the PDGFR-β pathway plays an important part in electrolyte homeostasis within the inner ear through maintaining the cochlear lateral wall.

Furthermore, due to the treatment with APB5, we found a defective sensory epithelium where PDGFR-β was little expressed. To determine whether the sensory epithelium could be affected by APB5, we also conducted *in situ* TUNEL analysis. In APB5-treated mice, cell death was extensively detectable not only in the mesenchymal tissue but also in the sensory epithelium of the cochlea and saccule. In the case of kidney glomeruli, no mesangial cells could be found in mice injected with APB5; and the apoptotic bodies were detected in the glomerular endothelial cells, which expressed PDGF-B. In the case of kidney development, since PDGFR-β is not expressed in the endothelial cells, the effects of blockade of PDGFR-β are thought to have caused glomerular endothelial cell apoptosis by inducing the loss of mesangial cells (Sano et al., 2002). Also, in the sensory epithelium of the inner ear, PDGFR-β was barely detected, and thus cell death in the sensory epithelium might have been secondarily induced by the loss of mesenchymal tissue in the inner ear. As a conjecture, we propose that mesenchymal tissue adjacent to the sensory epithelium may be involved in survival of the sensory epithelium via PDGFR-β signaling. Another possible explanation of the result is that impaired ion homeostasis by blockade of the PDGFR-β pathway in the inner ear caused cell death in the sensory epithelium. The aged mouse inner ear shows morphological alteration in the spiral ligament (Hequembourg and Liberman, 2001), similar to that seen in the APB5-treated mouse inner ear. As these fibrocytes in the spiral ligament disappear, ion homeostasis in the cochlea might be disrupted. Such putative abnormalities in local endolymph ion composition might lead ultimately to hair cell degeneration. In either explanation, cell death in the sensory epithelium, induced by blockade of the PDGFR-β signal in the inner ear, may be ascribed, not to a direct effect but rather an indirect effect of the antagonistic antibody, APB5, on the sensory epithelium.

Whereas, the incidence of cell death in the cochlea and saccule of mice injected with APB5 was significantly higher than that in the control mice, the utricle was less affected by the antibody. This difference within the inner ear may be ascribed to the maturity of the blood–labyrinth barrier (BLB). The function of the BLB resembles that of the blood–brain barrier and is associated with the endothelial cell transport system in which tight junctions exist and pinocytotic vesicles are active in the endothelial cells (Jahnke, 1980). We speculate that APB5 administered intraperitoneally reaches the inner ear through the general circulation and works by extravasation from capillaries. Our study indicated that cell death of the sensory epithelium began to occur at around 10 days after starting the administration of APB5. The BLB becomes mature by 14 days after birth in the rat cochlea, whereas the macromolecular transport system in the crista ampullaris of the rat matures between five and seven days (Suzuki

et al., 1998; Suzuki and Kaga, 1999). Although the permeability of the BLB in the utricle and saccule has not been definitely documented, these reports show that the maturity of the BLB differs according to the location in the inner ear. The results of our study do not conflict with Suzuki's report that the BLB reaches completion within 14 days after birth in the rat cochlea. If APB5 were administered systemically after postnatal day 14 by the same procedure, the adult mice might not display any abnormal histological phenotype in their cochlea. A limitation of our study is that systemic administration of the antibody is available only for neonatal mice having an immature BLB.

In conclusion, we have shown that mesenchymal tissue defects especially in the lateral wall of the cochlea and microvascular abnormalities in the inner ear of the neonatal mouse were caused by the administration of antagonistic anti-PDGFR-β monoclonal antibody and that blockade of the PDGFR-β pathway could also induce cell death in the sensory epithelium. However, PDGFR-β may be different in properties from fibroblast growth factor-2, insulin-like growth factor-1, and transforming growth factor-α, which directly stimulate proliferation of the utricular epithelial cells (Zheng et al., 1997). Our findings indicate that PDGFR-β may be required to promote the survival of mesenchymal tissue and capillaries in the neonatal mouse inner ear. Considering the near-contiguous expression of the ligand and its receptor and the cochlear lateral wall defects caused by blockade of PDGFR-β, PDGFR-β signaling can be implicated as acting indirectly to contribute to the survival of the sensory epithelium. The results of our present study add PDGF to the list of significant growth factors which act on the neonatal inner ear. Further investigation will be needed to examine the molecular mechanism underlying the regulation of PDGFR-β signaling related to the structure and function of the inner ear.

Acknowledgments

We appreciate the technical assistance of A. Inagaki and H. Aoki (Department of Tissue and Organ Development), and would also like to thank Dr. Ken-ichi Tezuka, Dr. Tsutomu Motohashi (Department of Tissue and Organ Development) and the members of the Department of Otolaryngology for their helpful discussions.

References

Basciani, S., Mariani, S., Arizzi, M., Brama, M., Ricci, A., Betsholtz, C., Bondjers, C., Ricci, G., Catizone, A., Galdieri, M., Spera, G., Gnessi, L., 2004. Expression of platelet-derived growth factor (PDGF) in the epididymis and analysis of the epididymal development in PDGF-A, PDGF-B, and PDGF receptor β deficient mice. Biol. Reprod. 70, 168–177.

Bergsten, E., Uutela, M., Li, X., Pietras, K., Ostman, A., Heldin, C.H., Alitalo, K., Eriksson, U., 2001. PDGF-D is a specific, protease-activated ligand for the PDGF beta-receptor. Nat. Cell Biol. 3, 512–516.

Betsholtz, C., 2004. Insight into the physiological functions of PDGF through genetic studies in mice. Cytokine Growth Factor Rev. 15, 215–228.

Boström, H., Willetts, K., Pekny, M., Levéen, P., Lindahl, P., Hedstrand, H., Pekna, M., Hellström, M., Gebre-Medhin, S., Schalling, M., Nilsson, M., Kurland, S., Törnell, J., Heath, J.K., Betsholtz, C., 1996. PDGF-A signaling is a critical event in lung alveolar myofibroblast development and alveogenesis. Cell 85, 863–873.

Davidson, J.M., Aquino, A.M., Woodward, S.C., Wilfinger, W.W., 1999. Sustained microgravity reduces intrinsic wound healing and growth factor responses in the rat. EMBO J. 13, 325–329.

Fruttiger, M., Calver, A.R., Krüger, W.H., Mudhar, H.S., Michalovich, D., Takakura, N., Nishikawa, S., Richardson, W.D., 1996. PDGF mediates a neuron-astrocyte interaction in the developing retina. Neuron 17, 1117–1131.

Fruttiger, M., Karlsson, L., Hall, A.C., Abramsson, A., Calver, A.R., Bostrom, H., Willetts, K., Bertold, C.H., Heath, J.K., Betsholtz, C., Richardson, W.D., 1999. Defective oligodendrocyte development and severe hypomyelination in PDGF-A knockout mice. Development 126, 457–467.

Fruttiger, M., Calver, A.R., Richardson, W.D., 2000. Platelet-derived growth factor is constitutively secreted from neuronal cell bodies but not from axons. Curr. Biol. 10, 1283–1286.

Gnessi, L., Basciani, S., Mariani, S., Arizzi, M., Spera, G., Wang, C., et al., 2000. Leydig cell loss and spermatogenic arrest in platelet-derived growth factor (PDGF)-A-deficient mice. J. Cell Biol. 149, 1019–1026.

Heldin, C.H., Wasteson, A., Westermark, B., 1985. Platelet-derived growth factor. Mol. Cell Endocrinol. 39, 169–187.

Heldin, C.H., Ostman, A., Ronnstrand, L., 1998. Signal transduction via platelet-derived growth factor receptors. Biochim. Biophys. Acta 1378, F79–F113.

Heldin, C.H., Westermark, B., 1999. Mechanism of action and in vivo role of platelet-derived growth factor. Physiol. Rev. 79, 1283–1296.

Hellström, M., Kalén, M., Lindahl, P., Abramsson, A., Betsholtz, C., 1999. Role of PDGF-B and PDGFR-beta in recruitment of vascular smooth muscle cells and pericytes during embryonic blood vessel formation in the mouse. Development 126, 3047–3055.

Hellström, M., Gerhardt, H., Kalén, M., Li, X., Eriksson, U., Wolburg, H., Betsholtz, C., 2001. Lack of pericytes leads to endothelial hyperplasia and abnormal vascular morphogenesis. J. Cell Biol. 153, 543–553.

Hequembourg, S., Liberman, M.C., 2001. Spiral ligament pathology: a major aspect of age-related cochlear degeneration in C57BL/6 mice. J. Assoc. Res. Otolaryngol. 2, 118–129.

Hoch, R.V., Soriano, P., 2003. Roles of PDGF in animal development. Development 130, 4769–4784.

Jahnke, K., 1980. The blood-perilymph barrier. Arch. Otorhinolaryngol. 228, 29–34.

Kamiya, K., Fujinami, Y., Hoya, N., Okamoto, Y., Kouike, H., Komatsuzaki, R., Kusano, R., Nakagawa, S., Satoh, H., Fujii, M., Matsunaga, T., 2007. Mesenchymal stem cell transplantation accelerates hearing recovery through the repair of injured cochlear fibrocytes. Am. J. Pathol. 171, 214–226.

Karlsson, L., Bondjers, C., Betsholtz, C., 1999. Roles for PDGF-A and sonic hedgehog in development of mesenchymal components of the hair follicle. Development 126, 2611–2621.

Karlsson, L., Lindahl, P., Heath, J.K., Betsholtz, C., 2000. Abnormal gastrointestinal development in PDGF-A and PDGFR-(alpha) deficient mice implicates a novel mesenchymal structure with putative instructive properties in villus morphogenesis. Development 127, 3457–3466.

LaRochelle, W.J., Jeffers, M., McDonald, W.F., Chillakuru, R.A., Giese, N.A., Lokker, N.A., Sullivan, C., Boldog, F.L., Yang, M., Vernet, C., Burgess, C.E., Fernandes, E., Deegler, L.L., Rittman, B., Shimkets, J., Shimkets, R.A., Rothberg, J.M., Lichenstein, H.S., 2001. PDGF-D, a new protease-activated growth factor. Nat. Cell Biol. 3, 517–521.

Lee, Y.W., Ozeki, M., Juhn, S.K., Lin, J., 2004. Expression of platelet-derived growth factor in the developing cochlea of rats. Acta Otolaryngol. 124, 558–562.

Levéen, P., Pekny, M., Gebre-Medhin, S., Swolin, B., Larsson, E., Betsholtz, C., 1994. Mice deficient for PDGF B show renal, cardiovascular, and hematological abnormalities. Genes Dev. 8, 1875–1887.

Li, X., Ponten, A., Aase, K., Karlsson, L., Abramsson, A., Uutela, M., Backstrom, G., Hellström, M., Bostrom, H., Li, H., Soriano, P., Betsholtz, C., Heldin, C.H., Alitalo, K., Ostman, A., Eriksson, U., 2000. PDGF-C is a new protease-activated ligand for the PDGF alpha-receptor. Nat. Cell Biol. 2, 302–309.

Lindahl, P., Johansson, B.R., Levéen, P., Betsholtz, C., 1997a. Pericyte loss and microaneurysm formation in PDGF-B-deficient mice. Science 277, 242–245.

Lindahl, P., Karlsson, L., Hellström, M., Gebre-Medhin, S., Willetts, K., Heath, J.K., Betsholtz, C., 1997b. Alveogenesis failure in PDGF-A-deficient mice is coupled to lack of distal spreading of alveolar smooth muscle cell progenitors during lung development. Development 124, 3943–3953.

Lindahl, P., Hellström, M., Kalén, M., Karlsson, L., Pekny, M., Pekna, M., Soriano, P., Betsholtz, C., 1998. Paracrine PDGF-B/PDGF-R beta signaling controls mesangial cell development in kidney glomeruli. Development 125, 3313–3322.

Malgrange, B., Rogister, B., Lefebvre, P.P., Mazy-Servais, C., Welcher, A.A., Bonnet, C., Hsu, R.Y., Rigo, J.M., Van De Water, T.R., Moonen, G., 1998. Expression of growth factors and their receptors in the postnatal rat cochlea. Neurochem. Res. 23, 1133–1138.

Malgrange, B., Rigo, J.M., Coucke, P., Thiry, M., Hans, G., Nguyen, L., Van De Water, T.R., Moonen, G., Lefebvre, P.P., 2002. Identification of factors that maintain mammalian outer hair cells in adult organ of Corti explants. Hear. Res. 170, 48–58.

Ohlsson, R., Falck, P., Hellström, M., Lindahl, P., Boström, H., Franklin, G., Ahrlund-Richter, L., Pollard, J., Soriano, P., Betsholtz, C., 1999. PDGF-B regulates the development of the labyrinthine layer of the mouse fetal placenta. Dev. Biol. 212, 124–136.

Ramachandran, R.K., Wikramanayake, A.H., Uzman, J.A., Govindarajan, V., Tomlinson, C.R., 1997. Disruption of gastrulation and oral-aboral ectoderm differentiation in the Lytechinus pictus embryo by a dominant/negative PDGF receptor. Development 124, 2355–2364.

Raphael, Y., Altschuler, R.A., 2003. Structure and innervation of the cochlea. Brain Res. Bull. 60, 397–422.

Risau, W., Drexler, H., Mironov, V., Smits, A., Siegbahn, A., Funa, K., Heldin, C.H., 1992. Platelet-derived growth factor is angiogenic in vivo. Growth Factors 7, 261–266.

Saffer, L.D., Rende, G., Corwin, J.T., 1996. An RT-PCR analysis of mRNA for growth factor receptors in damaged and control sensory epithelia of rat utricles. Hear. Res. 94, 14–23.

Sano, H., Sudo, T., Yokode, M., Murayama, T., Kataoka, H., Takakura, N., Nishikawa, S., Nishikawa, S., Kita, T., 2001. Functional blockade of platelet-derived growth factor receptor-beta but not of receptor-alpha prevents vascular smooth muscle cell accumulation in fibrous cap lesions in apolipoprotein E-deficient mice. Circulation 103, 2955–2960.

Sano, H., Ueda, Y., Takakura, N., Takemura, G., Doi, T., Kataoka, H., Murayama, T., Xu, Y., Sudo, T., Nishikawa, S., Nishikawa, S.I., Fujiwara, H., Kita, T., Yokode, M., 2002. Blockade of platelet-derived growth factor receptor-β pathway induces

apoptosis of vascular endothelial cells and disrupts glomerular capillary formation in neonatal mice. Am. J. Pathol. 161, 135–143.
Soriano, P., 1994. Abnormal kidney development and hematological disorders in PDGF beta-receptor mutant mice. Genes Dev. 15, 1888–1896.
Soriano, P., 1997. The PDGF alpha receptor is required for neural crest cell development and for normal patterning of the somites. Development 124, 2691–2700.
Suzuki, M., Yamasoba, T., Kaga, K., 1998. Development of the blood-labyrinth barrier in the rat. Hear. Res. 116, 107–112.
Suzuki, M., Kaga, K., 1999. Development of blood-labyrinth barrier in the semicircular canal ampulla of the rat. Hear. Res. 129, 27–34.
Wangemann, P., 2002. K+ cycling and the endocochlear potential. Hear. Res. 165, 1–9.
Xiang, M., Gao, W.Q., Hasson, T., Shin, J.J., 1998. Requirement for Brn-3c in maturation and survival, but not in fate determination of inner ear hair cells. Development 125, 3935–3946.
Zheng, J.L., Helbig, C., Gao, W.Q., 1997. Induction of cell proliferation by fibroblast and insulin-like growth factor in pure rat inner ear epithelial cell cultures. J. Neurosci. 17, 216–226.

Biochemical and Biophysical Research Communications 380 (2009) 609–613

Contents lists available at ScienceDirect

Biochemical and Biophysical Research Communications

journal homepage: www.elsevier.com/locate/ybbrc

Identification and characterization of stem cell-specific transcription of *PSF1* in spermatogenesis

Yinglu Han, Masaya Ueno, Yumi Nagahama, Nobuyuki Takakura *

Department of Signal Transduction, Research Institute for Microbial Diseases, Osaka University, 3-1, Yamada-oka, Suita, Japan

ARTICLE INFO

Article history:
Received 22 January 2009
Available online 27 January 2009

Keywords:
DNA replication
Testis development
Promoter
PSF1
Stem cell

ABSTRACT

PSF1 is an evolutionarily conserved DNA replication factor, which forms the GINS complex with PSF2, PSF3, and SLD5. The mouse *PSF1* homolog has been identified from a stem cell-specific cDNA library. To investigate its transcriptional regulatory mechanisms during differentiation, we studied *PSF1* mRNA expression in testis and characterized its promoter. No canonical TATA or CAAT boxes could be found in the *PSF1* 5′-flanking region, whereas several consensus AML1, GATA, and Sry putative binding sequences are predicted within 5 kb of the putative transcription start site. In addition, binding sites for oncoproteins such as Myb and Ets were also found in the promoter. In testis, various *PSF1* gene transcription initiation sites are present and short transcripts encoding two novel isoforms, PSF1b and 1c, were found. However, spermatogonium stem cells specifically express transcripts for PSF1a. These data suggest that PSF1 is tightly regulated at the transcriptional level in stem cells.

Because of the finite life span of most mature cells, tissue stem cells, and progenitors are required to supply replacements by proliferation and differentiation. Particularly, testis and bone marrow (BM) stem cells continuously self-renew and also produce differentiated cell lineages. Hematopoietic stem cells (HSCs) and spermatogonial stem cells (SSCs) have a high regenerative capacity. In a mouse experimental model, one single HSC was found to be sufficient to reconstitute hematopoiesis when transplanted into a BM-ablated recipient [1]. When spermatogenesis is disrupted by high temperatures or drugs, surviving SSCs can regenerate spermatogenesis [2,3]. Because these tissue stem cells have great regenerative capacity for reconstituting ablated tissues, ex vivo amplification of stem cells without loss of self-renewal and multidifferentiation potential represents an important target for transplantation, gene, and cellular therapies. In order to study the molecular mechanisms regulating self-renewal of stem cells, knock-out (KO) mice lacking several cell cycle-related genes, such as p27, p18, and ATM, were generated as previously reported [4–6]. However, their downstream function in the self-renewal process, especially regarding molecules involved in DNA replication, is currently not known.

The initiation of DNA replication in eukaryotic cells is mediated by a highly ordered series of steps involving multiple complexes at replication origins [7,8]. This process commences with the binding of the origin recognition complex (ORC) to replication origins. CDC6 and Cdt1 bind to ORCs to act as loading factors for the Mcm2-7 (minichromosome maintenance) complex and then pre-replication complexes (pre-RC) are established. At the G1/S transition of the cell cycle, the pre-RCs are transformed into initiation complexes (ICs). Activation of MCM helicase activity requires the action of two protein kinases, DDK (Cdc7-Dbf4) and CDK (cyclin-dependent), as well as the participation of at least eight additional factors, including Mcm10, Cdc45, Dpb11, synthetic lethal with dpb11 mutant-2 (Sld2), Sld3, and GINS [9]. GINS was recently identified as a novel heterotetrameric complex from lower eukaryotes. It consists of four subunits, SLD5, PSF1, PSF2, and PSF3, each of approximately 200 amino acid residues highly conserved in all eukaryotes and essential for both the initiation and progression of DNA replication [10–12].

By using lower eukaryote models, multiple steps for progression of DNA replication are now well understood at the protein level, e.g. phosphorylation, degradation, and/or interaction processes; however, how these factors are activated or inactivated at the RNA level in mammalian tissues consisting of multiple cell lineages and cells in different phases of the cycle has not been elucidated. Previously, we cloned the mouse ortholog of *PSF1* and *SLD5* from an HSC-specific cDNA library or by two-hybrid screening of a cDNA library derived from embryos [13,14]. Transcription of *PSF1* is predominantly found in highly proliferative tissues, such as BM and testis. Loss of *PSF1* causes embryonic lethality around the implantation stage [13], with *PSF1* $^{-/-}$ embryos showing impaired proliferation of multipotent stem cells, i.e., the inner cell mass. However, the transcriptional regulation of *PSF1* in immature cells is not understood.

Abbreviations: GINS, Go-ichi-ni-san; PSF, partner of SLD5; SSCs, sperm stem cells; HSCs, hematopoietic stem cells

* Corresponding author. Fax: +81 6 6879 8314.
E-mail address: ntakaku@biken.osaka-u.ac.jp (N. Takakura).

0006-291X/$ - see front matter © 2009 Elsevier Inc. All rights reserved.
doi:10.1016/j.bbrc.2009.01.133

Here, we have isolated the 5′ promoter sequence of the *PSF1* gene to investigate regulatory mechanisms responsible for tissue-specific expression. We report an in silico analysis of the potential *cis*-regulatory elements in the *PSF1* promoter. In addition, we studied SSC-specific transcription initiation sites and multiple transcription initiation sites of *PSF1* in testis.

Materials and methods

Animals. ICR mice were purchased from Japan SLC (Shizuoka, Japan). All animal studies were approved by the Osaka University Animal Care and Use Committee.

In situ hybridization. cDNA fragments were amplified by PCR using the primer set 5′-GAA TTC AAA GCT TTG TAT GAA CAA AAC CAG-3′ and 5′-GTC GAC TCA GGA CAG CAC GTG CTC TAG AAC T-3′, followed by ligation into pT7 Blue Vector (Novagen Inc., Madison, WI, USA). These plasmids were used for probe synthesis. Antisense and sense cRNA probes were synthesized using digoxigenin (DIG)-RNA labeling kits with T7 RNA polymerase (Roche Diagnostics, Indianapolis, IN, USA). Hybridization was performed as previously described [15].

Cell culture. Colon 26 cells were maintained in DMEM medium containing 10% FBS, 100 IU penicillin and 100 μg/ml streptomycin. The cells were plated in 10 cm tissue culture dishes in 5% CO_2 and 95% air at 37 °C.

5′-Rapid amplification of cDNA ends (5′-RACE). 5′-RACE was performed as described previously [16]. In brief, we used the 5′ RACE System for Rapid Amplification of cDNA Ends (Invitrogen, Carlsbad, CA) according to the manufacturer's instructions. Total RNA was purified from whole testis, embryonic day (E) 10.5 embryos, colon 26 cells, and sorted cells (see below) by the guanidine-thiocyanate extraction method. Total RNA of sorted cells was purified using RNeasy Plus Mini Kits (Qiagen, Valencia, CA) according to manufacturer's instructions. *PSF1* transcripts were reverse-transcribed with Superscript II (Invitrogen) using the gene-specific primer PSF1GSP1 5′-GCA TGT CTG TCA ATT TAA-3′. The products were poly(C) tailed by terminal deoxynucleotidyl transferase and amplified by PCR, using an anchor primer and the gene-specific primer 5′-CGA AGC AAC CGG TCA TAC A-3′ (PSF1ANGSP1). The amplified products were subcloned into pT7 Blue vector (Novagen).

5′ End amplification of PSF1 cDNA using 5′ End oligo-capped cDNA library. CapSite cDNA (Nippon Gene., Toyama, Japan) from mouse testis and embryo (Day15) was used as a template for PCR with primer 1RC (Nippon gene., Toyama, Japan) corresponding to the oligoribonucleotide sequence ligated at the cap site and a *PSF1* gene-specific primer, 5′-CGA AGC AAC CGG TCA TAC A-3′ (PSF1ANGSP1) and the PCR product was then used as a template for the second round PCR with nested primers 2RC (Nippon Gene) and 5′-GCTATCGTGCAGCGTCTATT-3′ (PSF1ANGSP2). The amplified products were used for Southern blotting or purified, cloned and sequenced.

Southern blotting. Amplified 5′-ends of cDNA by 5′-RACE (see above) were separated on 0.8% agarose gels and transferred onto nylon membrane filters which were hybridized overnight at 60 °C in DIG Easy Hyb (Roche Diagnostics, Germany) with a digoxigenin-labeled *PSF1* cDNA probe. The hybridized probe was detected with alkaline phosphatase-conjugated antidigoxigenin antibodies using the DIG luminescent detection kit (Roche), following the manufacturer's instructions. The probe was prepared by using PCR DIG Probe Synthesis Kits (Roche) with primers: E11prb-2s (5′-AGC TGG TTG CTG GTG TTG TGC GAC-3′) and E11prb-2r (5′-CGA AAA CAA GAA ACG CTC AGA TGG G-3′).

Enrichment of SSCs. Isolation of SSCs was as previously reported [17]. Briefly, experimental cryptorchid testes were produced by suturing the testis fat pad to the abdominal wall at 7 weeks of age. After 2 or 3 months, testes were dissected and then digested with collagenase (Type IV, Sigma, St Louis, MO) at 32 °C for 15 min. The cells were next digested with DNase (Sigma) and trypsin (GIBCO) at 32 °C for 10 min. When most of the cells were dispersed, the action of trypsin was terminated by adding PBS containing 1% fetal bovine serum. Cell sorting was performed as described previously [18]. The antibody used for detection of SSCs was a FITC-conjugated anti-α6-integrin antibody (BD Biosciences, San Jose, CA). Control cells were stained with isotype-matched control antibodies. After the final wash, cells were resuspended in 2 ml of PBS/FBS containing 1 μg/ml propidium iodide for identification of dead cells. The stained cells were analyzed by FACS Calibur (Becton & Dickinson, New Jersey, USA), and sorted by JSAN (Bay Bioscience, Kobe, Japan).

Results and discussion

Proliferating germ cells express high levels of PSF1 transcripts

Previously we reported that *PSF1* transcripts are highly expressed in testis and BM [13]. In addition, immunohistochemistry also revealed the presence of PSF1 protein specifically in the spermatogonia, lining the outermost layer of the testis [13]. Here, to study the expression of *PSF1* mRNA in the testis, we performed in situ hybridization with an antisense-probe which hybridized to spermatogonia (arrow) and spermatocytes (arrowhead) (Fig. 1A). No obvious signals were recorded when using the sense-probe (Fig. 1B). These data indicate that stem cell-specific expression of PSF1 may be regulated at the transcriptional or post-transcriptional level, because although PSF1 protein could be detected in the spermatogonia this was not the case in spermatocytes [13].

Identification and characterization of PSF1 transcription initiation sites

In order to identify the *PSF1* promoter, we performed 5′-RACE analysis with *PSF1* gene-specific primers. Total RNA from testis, colon 26 cells, and whole embryo were reverse-transcribed (see Materials and methods). Although a single DNA band <372 bp in length was obtained after nested PCR of colon 26 and whole embryo, a broad band was amplified from testis cDNA (Fig. 1C,a). We also observed smaller transcripts in 5′ End amplificated cDNA of *PSF1* using 5′ End oligo-capped cDNA library from testis compared to that from embryo (Fig. 1C,b). To exclude that this was caused by degraded RNA in our sample, total RNA was visualized by Ethidum bromide (Fig. 1D). The quality of the RNA in each sample was essentially the same. Thus, the broad band seen in testis was not caused by RNA degradation. We then amplified each cDNA fragment, purified them and subcloned them for DNA sequencing. Here, the 5′-end of the longest cDNA fragment is defined as "+1" (Table 1, +1 5′-TGC ACT TCT ATT-3"). It was located 157 bp upstream of the first ATG.

Putative cis elements of the 5′-flanking regions of PSF1

To characterize the 5′-flanking region of PSF1, we analyzed putative transcription binding sites in silico (Fig. 3). The proximal 5′-flanking region of the *PSF1* gene lacks consensus CAAT or TATA boxes, but possesses consensus Sp1 binding sites, which are characteristic of TATA-less gene promoters [19]. In the 5′-flanking region of *PSF1*, several putative *cis*-acting elements were identified, such as E2F, GATA, Myb, AML1, Evi-1, and Sry.

As previously reported, E2F is known to regulate DNA replication, cell cycle progression, DNA repair, and differentiation

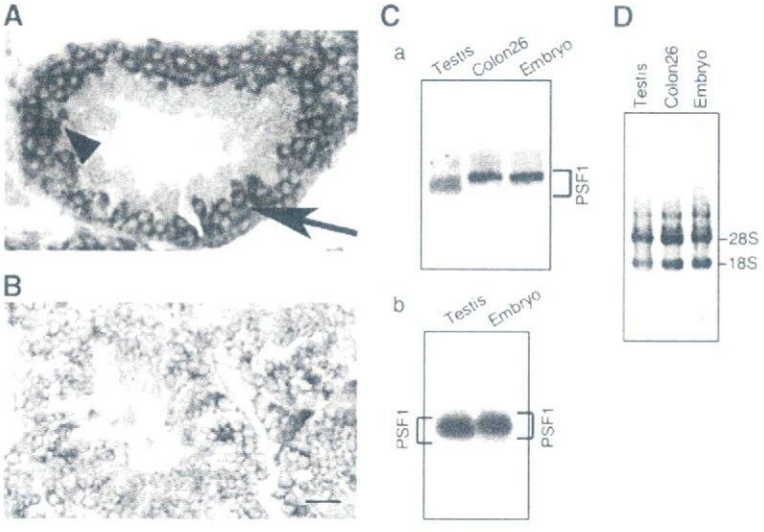

Fig. 1. *PSF1* expression in adult testis. (A) Antisense or (B) sense-probes for detection of *PSF1* were hybridized on sections of adult testis. Arrow, spermatogonia; arrowhead, spermatocyte. Bar indicates 20 μm. (C) Southern blot analysis of 5′-RACE product (a) and 5′ End amplificated cDNA of *PSF1* using 5′ End oligo-capped cDNA library (b) hybridized with a *PSF1* cDNA probe. Note that diffuse short bands are found in testis. (D) Ethidium bromide staining of total RNAs used in (C).

Table 1
Positions of 5′-RACE products of PSF1 transcripts.

Tissue or cells	Position of 5′-end	Translation		
		PSF1a	PSF1b	PSF1c
Colon 26	1, 20, 20, 20, 30, 30, 37, 42, 70, 70, 74, 227	92	0	8
Embryo	20, 30, 30, 30, 32, 35, 38, 47, 49, 50, 53, 57, 66, 72, 73, 117, 160	94	6	0
Testis	16, 22, 24, 25, 28, 28, 30, 30, 36, 66, 70, 70, 70, 70, 71, 73, 73, 73, 100, 107, 107, 113, 113, 113, 113, 113, 121, 130, 130, 146, 155, 155, 155, 161, 165, 165, 165, 165, 165, 165, 178, 178, 182, 182, 182, 182, 182, 186, 191, 193, 193, 193, 193, 213, 227, 230	59	13	28
SSCs	ND[a]	100[b]	0[b]	0[b]

[a] ND, No data.
[b] Percents are determined by PCR.

[20,21]. Moreover, E2F-1 is expressed in $CD34^+$ human hematopoietic stem and progenitor cells [22], and may play a critical role in hematopoiesis. Myb, AML1, and Evi-1 are also essential for HSC development [23–25]. GATA-1 does have a critical role in fate decision of HSCs [26]. Although GATA-2 has been suggested to play a role in maintenance of HSCs from the observation of GATA-2 $^{-/-}$ mice [27], it remains indeterminate whether GATA-2 enhances or suppresses the growth of HSCs [28–31]. As high level expression of PSF1 is observed in hematopoietic organs and testis in the adulthood, suggesting that these transcription factors may contribute to stem cell-specific transcription in testis as well as hematopoietic organs.

Multiple translation initiation sites

In our 5′-RACE analysis, small cDNA fragments were found specifically in testis (Fig. 2 and Table 1). Therefore, we next analyzed the translation initiation sites of each cDNA fragment (Fig. 3 and Table 1). ATG was present first in most of the transcripts tested in colon 26 and whole embryo, suggesting that these are translated to full-length PSF1 (PSF1a). However, in testis, there were many short transcripts which may be translated to truncated forms of PSF1 (PSF1b or PSF1c). Putative PSF1b lacks 6 amino acid residues and putative PSF1c lacks a partial portion of a coiled-coil domain compared to the PSF1 protein. The DNA sequences from the RT–PCR products of 5′ End amplifications using 5′ End oligo-capped cDNA library showed that 1.2% of the transcripts derived from testis were PSF1a type and the remnants were PSF1b and PSF1c. On the other hand, transcripts derived from embryo were almost exclusively PSF1a type. These data suggest that the short PSF1 transcripts may be translated into the truncated forms PSF1b and PSF1c specifically in testis.

SSCs express only the PSF1a isotype

Next, to investigate which RNAs are transcribed in sperm stem cells (SSCs, spermatogonia), we sorted these cells (Fig. 4A) and performed 5′-RACE analysis (Fig. 4B and Table 1). In contrast to whole testis, only one band was amplified from SSCs. After purification, we assessed the cDNA using PCR and found that amplificates contained ATG first, suggesting that only PSF1a is expressed in SSCs (Table 1).

We detected PSF1 protein in spermatogonia but not in spermatocytes by immunohistochemical analysis [13], although in situ hybridization revealed that primary and secondary spermatocytes as well as spermatogonia contained PSF1 transcripts. We found that SSCs express PSF1a but not PSF1b or PSF1c. These results suggest that the PSF1b and 1c RNA which is present in primary and secondary spermatocytes may be unstable and degrade easily.

In summary, we identified several *PSF1* transcription initiation sites. Various small cDNA fragments of *PSF1* were derived from testis, suggesting that *PSF1* RNAs are translated into three isotypes. These alternative forms may generate functionally different PSF1 proteins, contributing to differences in the mechanism of prolifer-

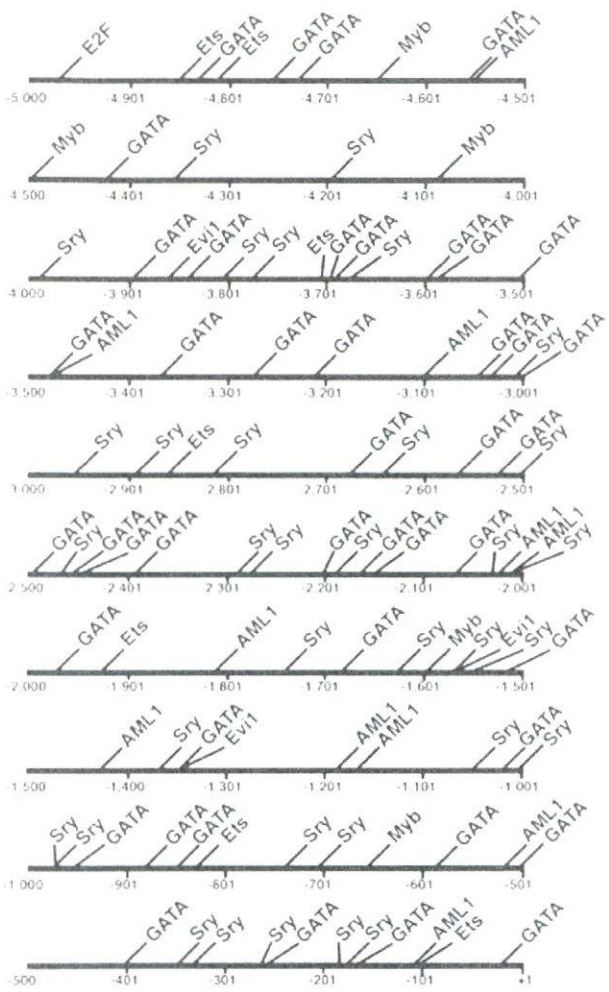

Fig. 2. Schematic representation of the putative transcriptional regulatory elements in the 5′-flanking region of the mouse *PSF1* gene. Consensus sequences of *cis*-regulatory elements in the *PSF1* promoter were sought in the TFSEARCH database (http://mbs.cbrc.jp/research/db/TFSEARCH.html). The numbers in parentheses indicate the positions of the first and last nucleotides of the elements.

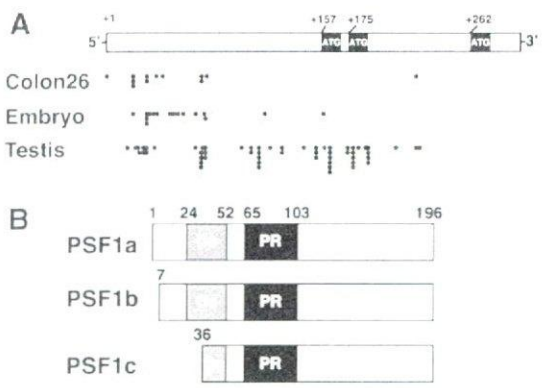

Fig. 3. Transcription initiation sites of *PSF1* and PSF1 isoforms. (A) Schematic representation of the summed data on transcription initiation sites. Each closed dot indicates the position of 5′-ends of 5′-RACE products. (B) Putative primary structures of PSF1 isoforms. Cc, N terminal region containing coiled-coil domain; PR, central region containing arginine-rich domain.

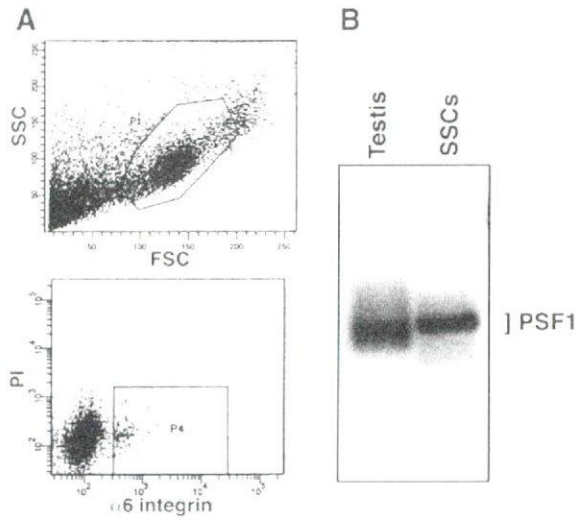

Fig. 4. Expression of *PSF1* gene in SSCs. (A) Flow cytometric analysis for sorting SSCs. Gated region for SSCs in SSC/FSC (upper) and α6-integrin$^+$ PI$^-$ cells population (lower) is shown. (B) Southern blot analysis of 5′-RACE products hybridized with a *PSF1* cDNA probe. Diffuse short bands were found in whole testis (Testis). SSCs, spermatogonium stem cells.

ation control in stem cells and progenitor cells. Further analysis of the regulatory mechanisms influencing PSF1 expression are needed to shed more light on the complex mechanisms of "stemness" in mammalian cells.

Acknowledgments

We thank N. Fujimoto, Y. Shimizu, K. Ishida, M. Sato, and Y. Nakano for technical assistance. We also thank K. Fukuhara for secretarial assistance. This work was partly supported by the Japanese Ministry of Education, Culture, Sports, Science and Technology, and the Japan Society for Promotion of Science.

References

[1] M. Osawa, K. Hanada, H. Hamada, H. Nakauchi, Long-term lymphohematopoietic reconstitution by a single CD34-low/negative hematopoietic stem cell, Science 273 (1996) 242–245.
[2] Y. Nishimune, S. Aizawa, T. Komatsu, Testicular germ cell differentiation in vivo, Fertil. Steril. 29 (1978) 95–102.
[3] C.J. van Keulen, D.G. de Rooij, Spermatogonial stem cell renewal in the mouse. II. After cell loss, Cell Tissue Kinet. 6 (1973) 337–345.
[4] T. Cheng, Rodrigues N.S. Stier, D.T., Scadden, Stem cell repopulation efficiency but not pool size is governed by p27 (kip1), Nat. Med. 6 (2000) 1235–1240.
[5] Y. Yuan, H. Shen, D.S. Franklin, D.T. Scadden, T. Cheng, In vivo self-renewing divisions of haematopoietic stem cells are increased in the absence of the early G1-phase inhibitor, p18INK4C, Nat. Cell Biol. 6 (2004) 436–442.
[6] K. Ito, A. Hirao, F. Arai, S. Matsuoka, K. Takubo, I. Hamaguchi, K. Nomiyama, K. Hosokawa, K. Sakurada, N. Nakagata, Y. Ikeda, T.W. Mak, T. Suda, Regulation of oxidative stress by ATM is required for self-renewal of haematopoietic stem cells, Nature 431 (2004) 997–1002.
[7] J.J. Blow, A. Dutta, Preventing re-replication of chromosomal DNA, Nat. Rev. Mol. Cell Biol. 6 (2005) 476–486.
[8] T.S. Takahashi, D.B. Wigley, J.C. Walter, Pumps, paradoxes and ploughshares: mechanism of the MCM2–7 DNA helicase, Trends Biochem. Sci. 30 (2005) 437–444.
[9] K. Labib, A. Gambus, A key role for the GINS complex at DNA replication forks, Trends Cell Biol. 17 (2007) 271–278.
[10] M. Kanemaki, A. Sanchez-Diaz, A. Gambus, K. Labib, Functional proteomic identification of DNA replication proteins by induced proteolysis in vivo, Nature 423 (2003) 720–724.
[11] Y. Kubota, Y. Takase, Y. Komori, Y. Hashimoto, T. Arata, Y. Kamimura, H. Araki, H. Takisawa, A novel ring-like complex of Xenopus proteins essential for the initiation of DNA replication, Genes Dev. 17 (2003) 1141–1152.
[12] Y. Takayama, Y. Kamimura, M. Okawa, S. Muramatsu, A. Sugino, H. Araki, H. Takisawa, GINS, a novel multiprotein complex required for chromosomal DNA replication in budding yeast, Genes Dev. 17 (2003) 1153–1165.